



THE UNIVERSITY *of* EDINBURGH

Edinburgh Research Explorer

Human brain-derived A oligomers bind to synapses and disrupt synaptic activity in a manner that requires APP

Citation for published version:

Wang, Z, Jackson, R, Hong, W, Taylor, WM, Corbett, GT, Moreno, A, Liu, W, Li, S, Frosch, MP, Slutsky, I, Young-Pearse, T, Spires-Jones, T & Walsh, DM 2017, 'Human brain-derived A oligomers bind to synapses and disrupt synaptic activity in a manner that requires APP' Journal of Neuroscience. DOI: 10.1523/JNEUROSCI.2009-17.2017

Digital Object Identifier (DOI):

[10.1523/JNEUROSCI.2009-17.2017](https://doi.org/10.1523/JNEUROSCI.2009-17.2017)

Link:

[Link to publication record in Edinburgh Research Explorer](#)

Document Version:

Peer reviewed version

Published In:

Journal of Neuroscience

General rights

Copyright for the publications made accessible via the Edinburgh Research Explorer is retained by the author(s) and / or other copyright owners and it is a condition of accessing these publications that users recognise and abide by the legal requirements associated with these rights.

Take down policy

The University of Edinburgh has made every reasonable effort to ensure that Edinburgh Research Explorer content complies with UK legislation. If you believe that the public display of this file breaches copyright please contact openaccess@ed.ac.uk providing details, and we will remove access to the work immediately and investigate your claim.



The Journal of Neuroscience

<https://jneurosci.msubmit.net>

JN-RM-2009-17R1

Human brain-derived A β oligomers bind to synapses and disrupt synaptic activity in a manner that requires APP

Dominic Walsh, Harvard Institutes of Medicine

Zemin Wang, Brigham and Women's Hospital and Harvard Medical School

Rosemary Jackson, University of Edinburgh

Wei Hong, Brigham and Women's Hospital and Harvard Medical School

Walter Taylor, Brigham and Women's Hospital and Harvard Medical School

Grant Corbett, Brigham and Women's Hospital, Harvard Medical School

Arturo Moreno, UCSF

Wen Liu, Brigham and Women's Hospital and Harvard Medical School

Shaomin Li, Brigham and Women's Hospital and Harvard Medical School

Matthew Frosch, Massachusetts General Hospital

Tracy Young-Pearse, Brigham and Women's Hospital, Harvard Medical School

and Ann Romney Center for Neurologic Diseases

Inna Slutsky, Tel Aviv University

Tara Spire-Jones, University of Edinburgh

Commercial Interest:

1 **Human brain-derived A β oligomers bind to synapses and**
2 **disrupt synaptic activity in a manner that requires APP**

3
4 Zemin Wang¹, Rosemary J. Jackson², Wei Hong¹, Walter M. Taylor¹, Grant T. Corbett¹,
5 Arturo Moreno¹, Wen Liu¹, Shaomin Li¹, Matthew P. Frosch³, Inna Slutsky⁴, Tracy
6 Young-Pearse¹, Tara L. Spires-Jones², and Dominic M. Walsh^{1*}

7
8 ¹Laboratory for Neurodegenerative Research, Ann Romney Center for Neurologic
9 Diseases, Brigham and Women's Hospital and Harvard Medical School, Boston, MA
10 02115, USA; ²The University of Edinburgh, UK Dementia Research Institute, 1 George
11 Square, Edinburgh, UK; ³Massachusetts General Institute for Neurodegenerative
12 Disease, Massachusetts General Hospital and Harvard Medical School, Charlestown,
13 MA 02129, USA; and ⁴Department of Physiology and Pharmacology, Sackler Faculty of
14 Medicine, Tel Aviv University; 69978 Tel Aviv, Israel.

15
16 *Correspondence to dwalsh3@bwh.harvard.edu

17
18 Running title: A β -mediated disruption of synaptic activity requires APP.

19
20 Number of Pages: 63

21 Number of Figures: 11

22 Number of Tables: 1

23 Number of words for Abstract: 161

24 Number of words for Introduction: 652

25 Number of words for Discussion: 1387

26

27 **Acknowledgments**

28 We thank Dr. Tiernan T. O'Malley for useful discussions and technical advice. This
29 work was supported by grants to DMW from the National Institutes of Health
30 (AG046275), Bright Focus, and the United States-Israel Binational Science Foundation
31 (2013244, DMW and IS); grants to TSJ from Alzheimer's Research UK and the Scottish
32 Government (ARUK-SPG2013-1), Wellcome Trust-University of Edinburgh Institutional
33 Strategic Support funds, and the H2020 European Research Council (ALZSYN); and to
34 the Massachusetts Alzheimer's Disease Research Center (AG05134). TSJ is a
35 member of the FENS Kavli Network of Excellence.

36

37 **Abstract**

38 Compelling genetic evidence links the amyloid precursor protein (APP) to Alzheimer's
39 disease (AD), and several theories have been advanced to explain the involvement of
40 APP in AD. A leading hypothesis proposes that a small amphipathic fragment of APP,
41 the amyloid β -protein ($A\beta$), self-associates to form soluble aggregates which impair
42 synaptic and network activity. Here, we employed the most disease-relevant form of $A\beta$,
43 protein isolated from AD brain. Using this material, we show that the synaptotoxic
44 effects of $A\beta$ depend on expression of APP and that the $A\beta$ -mediated impairment of
45 synaptic plasticity is accompanied by pre-synaptic effects which disrupt the
46 excitatory/inhibitory (E/I) balance. The net increase in the E/I ratio, and inhibition of
47 plasticity are associated with $A\beta$ localizing to synapses and binding of soluble $A\beta$
48 aggregates to synapses requires the expression of APP. Taken together, our findings
49 indicate a role for APP in AD pathogenesis beyond the generation of $A\beta$ and suggest
50 modulation of APP expression as a therapy for AD.

51

52 **Significance Statement**

53 Here, we report on the plasticity-disrupting effects of A β isolated from AD brain and the
54 requirement of APP for these effects. We show that A β -containing AD brain extracts
55 block hippocampal long-term potentiation (LTP), augment glutamate release probability
56 and disrupt the excitation/inhibition balance. Notably, these effects are associated with
57 A β localizing to synapses, and genetic ablation of APP prevents both A β binding and
58 A β -mediated synaptic dysfunctions. Our results emphasize the importance of APP in
59 AD and should stimulate new studies to elucidate APP-related targets suitable for
60 pharmacological manipulation.

61

62 **Introduction**

63 Mutation, over-expression or altered processing of the amyloid precursor protein (APP)
64 underlie all known monogenic cases of familial Alzheimer's disease (fAD) (Tanzi, 2012;
65 Guerreiro and Hardy, 2014). Although the physiological roles of APP are not fully
66 understood, a myriad of studies indicate that APP plays a role in synaptic plasticity,
67 dendritic morphogenesis, and neuroprotection (Muller and Zheng, 2012). Membrane-
68 tethered APP can act as a cell-adhesion molecule linking the pre-and post-synapse
69 (Soba et al., 2005) and APP has been shown to regulate synaptic vesicle proteins,
70 synaptic transmission and plasticity (Dawson et al., 1999; Lassek et al., 2013; Fanutza
71 et al., 2015; Lassek et al., 2016). In the rat dentate gyrus (DG), APP expression is
72 known to change during memory consolidation (Conboy et al., 2005) and
73 intraventricular administration of anti-APP antibodies or antisense oligonucleotides
74 results in profound amnesia (Doyle et al., 1990; Huber et al., 1993; Mileusnic et al.,
75 2000). Notably, APP is a component of the presynaptic GABA-B1a receptor (GABA_{B1a}-
76 R) complex (Bai et al., 2008; Schwenk et al., 2016) and neuron-type specific knock-out
77 of APP indicates an important role for APP in GABAergic transmission and maintenance
78 of the excitatory–inhibitory balance (Wang et al., 2014).

79 APP is a complex molecule that undergoes substantial post-translational modification
80 and processing as more than 10 different proteolytic fragments of APP have been
81 identified. Several of these are suggested to be pathogenic (Neve and McPhie, 2007;
82 Yankner and Lu, 2009; Tamayev et al., 2012; Welzel et al., 2014; Willem et al., 2015),
83 whereas others are neuroprotective (Mockett et al., 2017). The fragment from which the

84 precursor protein derives its name, the amyloid β -protein ($A\beta$), is found in the tell-tale
85 amyloid plaques which populate brains of individuals who die with AD. $A\beta$ comprises a
86 family of APP-derived peptides that share a common core of ~30 amino acids (Walsh
87 and Teplow, 2012) which are produced by the concerted action of two aspartyl
88 proteases, β -secretase and γ -secretase (De Strooper, 2010). $A\beta$ peptides are prone to
89 self-associate and multiple studies indicate that certain forms of $A\beta$ adversely affect
90 synaptic form and function (Li et al., 2009).

91 The synaptotoxic activity of $A\beta$ and the involvement of APP in synapse formation and
92 activity are particularly relevant to AD since *in vivo* and postmortem studies indicate that
93 synapse dysfunction and loss are prominent early features of AD (Scheff et al., 2006;
94 Scheff et al., 2007; Johnson et al., 2012). Acute studies in wild-type rodents show that
95 non-fibrillar, water-soluble $A\beta$ from a variety of sources are potent synaptotoxins
96 (Lambert et al., 1998; Walsh et al., 2002; Cleary et al., 2005; Lesne et al., 2006; Klyubin
97 et al., 2008; Minkeviciene et al., 2009; Kurudenkandy et al., 2014). Furthermore, *in vitro*
98 and *in vivo* studies demonstrate that the most disease-relevant form of non-fibrillar $A\beta$,
99 $A\beta$ extracted from the water-soluble phase of AD brain, inhibits long-term potentiation
100 (LTP), facilitates long-term depression (LTD), reduces synaptic remodeling, and impairs
101 memory consolidation (Shankar et al., 2008; Barry et al., 2011; Freir et al., 2011;
102 Borlikova et al., 2013; Jo et al., 2014; Yang et al., 2017). Here, we show that the block
103 of LTP mediated by $A\beta$ -containing AD brain extracts is accompanied by opposing
104 changes in excitatory and inhibitory pre-synaptic release probabilities and consequent
105 disruption of the excitation/inhibition (E/I) balance. The net increase in the E/I ratio and
106 inhibition of LTP require expression of APP and are associated with $A\beta$ localizing to

107 synapses. These findings suggest a link between A β toxicity and perturbation of the
108 normal regulatory role of APP, and are consistent with prior studies which have imputed
109 a role for APP in A β toxicity (White et al., 1998; Lorenzo et al., 2000; Shaked et al.,
110 2006; Sola Vigo et al., 2009; Fogel et al., 2014; Kirouac et al., 2017). In light of these
111 results we suggest that down-regulation of APP expression or modulation of its
112 interaction with synaptotoxic A β species should be investigated as an approach to treat
113 AD.

114

115 **Materials and Methods**

116 **Reagents**

117 All chemicals and reagents were purchased from Sigma-Aldrich unless otherwise noted.
118 Synthetic A β 1–42 was synthesized and purified using reverse-phase HPLC by Dr.
119 James I. Elliott at the ERI Amyloid laboratory (Oxford, CT, USA). Peptide mass and
120 purity (>99%) were confirmed by reverse-phase HPLC and electrospray/ion trap mass
121 spectrometry. N-terminally extended (NTE) -31A β -40 was prepared and purified as
122 described previously (Mc Donald et al., 2015) and recombinant Aeta-alpha (A η - α ,
123 APP₅₀₅₋₆₁₁) was a gift from Drs. Willem and Haass (Ludwig-Maximillan University,
124 Munich).

125

126 **Antibodies**

127 The antibodies used and their source are described in Table 1.

128

129 **Preparation of human brain extracts**

130 All human specimens were obtained and used in accordance with the Partner's
131 Institutional Review Board (Protocol: Walsh BWH 2011). Brain tissue was obtained
132 from 2 of individuals (referred to as AD1 and AD2) who died with AD and one individual
133 who died free of AD (designated NC). AD1 was an 87-year-old man who 9 months prior
134 to death had scored 23 on the MMSE and designated Braak stage 4 at postmortem had

135 pathological changes consistent with mild AD. AD2 was a 68-year-old female with end-
136 stage AD. Three years prior to death AD2 scored 23 on the MMSE, but in her last
137 weeks she was unable to answer questions other than to provide her first name. Upon
138 postmortem examination there was evidence of fulminant amyloid and neurofibrillary
139 tangle pathology which was designated Braak stage V/VI. Neither AD1 nor AD2 had a
140 family history of AD. NC was a 58-year-old female who died free of AD symptoms and
141 pathology. AD1 and NC has post-mortem intervals (PMI) of 18 hours, and AD had a
142 PMI of 12 hours. Aqueous extracts of brain were prepared by homogenizing cortical
143 tissue in a buffer which we refer to as artificial cerebrospinal fluid base buffer (aCSF-B)
144 (124 mM NaCl, 2.8 mM KCl, 1.25 mM NaH₂PO₄, 26 mM NaHCO₃, pH 7.4). aCSF-B is
145 the core buffer used in subsequent electrophysiology experiments. Whole frozen
146 temporal cortex was left at 4°C until the tissue was sufficiently soft to cut. Meninges
147 and large blood vessels were removed and gray matter dissected from white matter.
148 The total amount of gray matter obtained was between 12-14 g. Two gram lots of tissue
149 were diced using a razor blade and then homogenized in 10 ml of ice-cold aCSF-B
150 (containing 5 mM Ethylenediaminetetraacetic acid, 1 mM Ethyleneglycoltetraacetic acid,
151 5 µg/ml Leupeptin, 5 µg/ml Aprotinin, 2 µg/ml Pepstatin, 120 µg/ml Pefabloc and 5 mM
152 NaF) with 25 strokes of a Dounce homogenizer (Fisher, Ottawa, Canada).
153 Homogenates from 6, 2 g lots were pooled and centrifuged at 198,000 g and 4°C for
154 110 minutes in a SW 41-Ti rotor (Beckman Coulter, Fullerton, CA). The upper 90% of
155 supernatant was dialyzed (using Slide-A-Lyzer™ G2 Dialysis Cassettes, 2K MWCO,
156 Fisher Scientific) against fresh aCSF-B to remove bioactive small molecules and drugs.
157 Dialysis was performed at 4°C against a 100-fold excess of buffer with buffer changed 3

158 times over a 36 hour period. Thereafter, extracts were divided into 2 parts: 1 portion
159 was immunodepleted (ID) of A β by 3 rounds of 12 hour incubations with the anti-A β
160 antibody, AW7, plus Protein A sepharose (PAS) beads at 4 °C (Freir et al., 2011). The
161 second portion was treated in an identical manner, but this time incubated with pre-
162 immune serum plus PAS beads. Samples were cleared of beads and 0.5 ml aliquots
163 stored at -80°C until used for biochemical or electrophysiological experiments. Samples
164 were thawed only once prior to use.

165

166 **Preparation of amyloid-derived diffusible ligands (ADDLs)**

167 Amyloid-derived diffusible ligands (ADDLs) were prepared essentially as described
168 previously (Freir et al., 2011). Hexafluoro-2-propanol (HFIP; 222 μ l) was added to 1 mg
169 of A β (1–42) in a 2 ml low-binding microcentrifuge tube to produce a peptide
170 concentration of 1 mM. The solution was split into two tubes, incubated at 37°C for 1
171 hour and mixed by vortexing every 10 minutes. The HFIP was gently evaporated under
172 a nitrogen stream with rotation of the tube to ensure formation of an even film of peptide
173 on the lower walls of the tube. Dried peptide films were stored over desiccant at 20°C
174 for a minimum of 14 hours. The peptide film from each tube was then dissolved in 20 μ l
175 of anhydrous DMSO (Life Technologies, Woburn, MA) and 5 μ l lots of the DMSO
176 mixture was added stepwise to 980 μ l of F-12 medium (Life Technologies), with
177 vortexing between each addition. The resulting solution was incubated at 4°C for 48
178 hours and then centrifuged at 16,000 g for 10 minutes. The upper 95% of the
179 supernatant was transferred to a new microcentrifuge tube and the protein

180 concentration determined using the extinction coefficient, $\epsilon_{275} = 1361 \text{ M}^{-1} \text{ cm}^{-1}$ (O'Malley
181 et al., 2014). Aliquots were then immediately frozen on dry ice and stored at -80°C .

182

183 **Characterization of ADDLs**

184 The size and morphology of structures present in the ADDLs preparation were
185 investigated using negative contrast electron microscopy and analytical size exclusion
186 chromatography (SEC). Samples were stained and visualized essentially as described
187 previously (Betts et al., 2008). An aliquot of the ADDL preparation (50 μl) was diluted
188 1:1 with F12 media and then adsorbed (10 μl) onto formvar-coated copper grids
189 (Electron Microscopy Sciences). After 1 minute, 10 μl 0.25% glutaraldehyde was added
190 and incubated for 1 minute. Thereafter, grids were wicked dry using filter paper,
191 washed twice with MilliQ water and then stained with 1% uranyl-acetate for 2 minutes.
192 Grids were allowed to air dry for at least 10 minutes, stored at room temperature and
193 then examined using a 1200EX microscope (JEOL).

194 A separate aliquot of ADDLs (50 μl) was thawed and loaded on to a Superdex 75
195 3.2/300 PE column (GE Healthcare) eluted in PBS pH 7.4 at 0.8 ml/min using a
196 Shimadzu HPLC system.

197

198 **Preparation of synthetic peptides used for Western blotting**

199 $\text{A}\eta\alpha$ peptide was dissolved in 50 mM ammonium bicarbonate, pH 8.5, diluted to 10
200 ng/ μl , aliquoted and stored frozen at -80°C . $\text{A}\beta_{1-42}$ and $\text{-31A}\beta_{40}$ which are prone to
201 aggregate were treated to depolymerize any pre-existing aggregates. Briefly, peptides
202 were dissolved in 50 mM Tris-HCl, pH 8.5, containing 7 M guanidium-HCl (GuHCl) and

203 5 mM ethylenediaminetetraacetic acid (EDTA) at a concentration of 1 mg/ml and
204 incubated at room temperature (RT) overnight. Samples were then centrifuged for 30
205 minutes at 16,000 *g* and chromatographed on a Superdex 75 10/300 column eluted at
206 0.5 ml/min with 50 mM ammonium bicarbonate, pH 8.5. The concentration of the peak
207 fraction for each sample was determined by absorbance at 275 nm. The peptide was
208 then diluted to 10 ng/ μ l, aliquoted and stored frozen at -80°C.

209

210 **Immunoprecipitation/Western blotting (IP/WB) of A β in brain extracts**

211 Extracts were first pre-cleared with PAS beads to minimize non-specific interactions in
212 the subsequent IP. One ml aliquots of extracts were incubated with 15 μ l PAS beads
213 for 1 hour at 4°C with gentle shaking. PAS beads were removed by centrifugation
214 (4000 *g* for 5 minutes) and the supernatant divided into 0.5 ml aliquots. Each aliquot
215 was incubated with 10 μ l of AW7 and 15 μ l PAS beads overnight at 4°C with gentle
216 shaking. A β -antibody-PAS complexes were collected by centrifugation and washed as
217 previously described (Shankar et al., 2011). The immunoprecipitated (IP'd) A β was
218 eluted by boiling in 18 μ l of 1 \times sample buffer (50 mM Tris, 2% w/v SDS, 12% v/v
219 glycerol with 0.01% phenol red) and electrophoresed on hand poured, 15 well 16%
220 polyacrylamide tris-tricine gels. A η - α , A β 1-42 and -31A β 40 were run as loading
221 controls and protein transferred onto 0.2 μ M nitrocellulose at 400 mA and 4°C for 2
222 hour. Blots were microwaved in PBS and A β detected using the anti-A β 40 and anti-
223 A β 42 antibodies, 2G3 and 21F12, and bands visualized using a Li-COR Odyssey
224 infrared imaging system (Li-COR, Lincoln, NE). To determine if AW7 IP'd other APP

225 metabolites (e.g. APPs α , N-terminally extended A β or A η peptides) from AD brain
226 extracts, certain blots were developed with 6E10 (Table 1).

227

228 **MSD A β immunoassays**

229 Samples were analyzed for A β content using 2 distinct assay formats: the A β x-42 assay
230 that preferentially detects A β 42 monomers and the oAssay that preferentially detects A β
231 oligomers and aggregates (Mably et al., 2015; Yang et al., 2015). Immunoassays were
232 performed using the Meso Scale Discovery (MSD) platform and reagents from Meso
233 Scale (Rockville, MD). The A β x-42 assay uses mAb m266 (3 μ g/ml) for capture and
234 biotinylated 21F12 (1 μ g/ml) for detection, and the oAssay uses mAb 1C22 (3 μ g/ml) for
235 capture and biotinylated 3D6 (1 μ g/ml) for detection. Samples, standards and blanks
236 were loaded in duplicate and analyzed as described previously (Mably et al., 2015).

237 Since [Guanidine Hydrochloride](#) (GuHCl) effectively disaggregates high molecular weight
238 A β species (Mably et al., 2015), samples were analyzed both with and without
239 incubation in 5 M GuHCl. Analysis of samples in the absence of GuHCl allows the
240 measurement of native A β 42 monomer using the A β x-42 assay, and native A β
241 aggregates using the oAssay. Analysis of samples treated with GuHCl allows detection
242 of disassembled aggregates with A β x-42 assay. To dissociate aggregates, 20 μ l of
243 extract was incubated overnight with 50 μ l of 7 M GuHCl at 4°C. Thereafter samples
244 were diluted 1:10 with assay diluents so that the final GuHCl concentration was 0.5 M.
245 A β standards were prepared in tris-buffered saline (TBS), pH 7.4 containing 0.5 M

246 GuHCl, 0.05% Tween 20 and 1% Blocker A so that both standards and samples
247 contained the same final concentration of GuHCl.

248

249 **Mice**

250 All animal procedures were performed in accordance with the National Institutes of
251 Health Policy on the Use of Animals in Research and were approved by the Harvard
252 Medical School Standing Committee on Animals. Wild-type (WT) C57BL/6 mice were
253 purchased from the Jackson Laboratory (Bar Harbor, ME). APP KO mice on a C57BL/6
254 background and littermate WT controls were obtained from the Young-Pearse lab
255 (Callahan et al., 2017). A second line of APP KO mice were purchased from the
256 Jackson Laboratory (APP^{tm1^{Db}o}/J, The Jackson Laboratory, Bar Harbor, ME) (Zheng et
257 al., 1995) and for certain experiments these animals were bred with WT C57BL/6 mice
258 to generate APP (+/-) hemizygotes. Animals were housed in a room with a 12 hour
259 light/dark circadian cycle with *ad libitum* access to food and water. Mice were
260 genotyped by PCR prior to use, and both male and female mice were used. In certain
261 experiments, upon completion of electrophysiological recordings, brain slices were used
262 for Western blotting or array tomography.

263

264 **Brain slice preparation**

265 Two to three months old male and female animals were anaesthetized with isoflurane
266 and decapitated. Brains were rapidly removed and immediately immersed in ice-cold

267 (0-4°C) artificial cerebrospinal fluid (aCSF). The aCSF contained (in mM): 124 NaCl, 3
268 KCl, 2.4 CaCl₂, 2 MgSO₄·7H₂O, 1.25 NaH₂PO₄, 26 NaHCO₃ and 10 D-glucose, and was
269 equilibrated with 95% O₂ and 5% CO₂, pH 7.4, 310 mOsm. Coronal brain slices (350
270 μm), including hippocampus (Wang et al., 2008), were prepared using a Leica VT1000
271 S vibratome (Leica Biosystems Inc, Buffalo Grove, IL), transferred to an interface
272 chamber and incubated at 34 ± 5°C for 20 minutes and then kept at room temperature
273 for 1 hour before recording.

274

275 **Long-term potentiation (LTP) recording**

276 Brain slices were transferred to a submerged recording chamber and perfused (10
277 ml/min) with oxygenated (95% O₂ and 5% CO₂) aCSF 10 minutes before
278 electrophysiological recordings. Brain slices were visualized using an infrared and
279 differential interference contrast camera (IR-DIC camera, Hitachi, Japan) mounted on
280 an upright Olympus microscope (Olympus, Tokyo, Japan). Recording electrodes were
281 pulled from borosilicate glass capillaries (Sutter Instruments, Novato, CA) using a
282 micropipette puller (Model P-97; Sutter Instruments, Novato, CA) with resistance ~2 MΩ
283 when filled with aCSF. To induce field excitatory post-synaptic potentials (fEPSPs) in
284 the hippocampal CA1, a tungsten wire stimulating electrode (FHC, Inc., Bowdoin, ME)
285 was placed on the Schaffer collaterals of the CA3 and a recording electrode was placed
286 at least 300 μm away on the striatum radiatum of the CA1. The initial 10-40 % slope of
287 fEPSPs were calculated. Test stimuli were delivered once every 20 seconds (0.05 Hz)
288 and the stimulus intensity was adjusted to produce a baseline fEPSP of 30–40% of the
289 maximal response. A stable baseline was recorded for at least 10 minutes prior to

290 addition of sample. Thirty minutes following application of sample, LTP was induced by
291 theta burst stimulation (TBS). This involved 3 trains, each of 4 pulses delivered at 100
292 Hz, 10 times, with an interburst interval of 200 milli-second with a 20 second interval
293 between each train. Field potentials were recorded using a Multiclamp amplifier
294 (Multiclamp 700B; Molecular Devices, Sunnyvale, CA) coupled to a Digidata 1440A
295 digitizer. Signal was sampled at 10 kHz and filtered at 2 kHz and data were analyzed
296 using Clampex 10 software (Molecular Devices, Sunnyvale, CA).

297

298 **Whole-cell patch clamp recording**

299 Brain slices were prepared from male and female WT and APP KO mice (1-2 months
300 old) as described above for LTP experiments but using a cutting solution that contained
301 sucrose (in mM: 72 sucrose, 83 NaCl, 2.5 KCl, 1 NaH₂PO₄, 3.3 MgSO₄·7H₂O, 26.2
302 NaHCO₃, 22 dextrose, and 0.5 CaCl₂) saturated with 95% O₂ and 5% CO₂, pH 7.4, 310
303 mOsm (Wang et al., 2015). Slices were incubated in oxygenated slicing solution for 20
304 minute, and held at room temperature for a further 40 minute prior to recording. Slices
305 were transferred to a submerged recording chamber and perfused (10 ml/min) with
306 oxygenated (95% O₂ and 5% CO₂) aCSF for 30 minute at room temperature. Whole-
307 cell recordings were made from the somata of CA1 pyramidal neurons visualized using
308 an IR-DIC camera mounted on an upright Olympus microscope (Olympus, Tokyo,
309 Japan). Patch pipettes (4–7MΩ) were filled with an internal solution containing (in mM):
310 120 CsGluconate, 5 MgCl₂, 0.6 EGTA, 30 HEPES, 4 MgATP, 0.4 Na₂GTP, 10
311 phosphocreatine-Tris, 5 N-(2,6-Dimethylphenylcarbamoylmethyl)triethylammonium
312 bromide (QX-314); 290 mOsm; pH was adjusted to 7.2 with CsOH. Signal was

313 acquired using a Multiclamp amplifier (Multiclamp 700B; Molecular Devices, Sunnyvale,
314 CA) with Clampex 10 software (Molecular Devices, Sunnyvale, CA), sampled at 10 kHz
315 and filtered at 2 kHz. Data were stored on a PC after digitization by an A/D converter
316 (Digidata 1440A, Molecular Devices, Sunnyvale, CA) for offline analysis. Membrane
317 potential was corrected for the liquid junction potential of 13.7 mV. Neurons with
318 negative resting membrane potential less than -60 mV were not analyzed. Input
319 resistance and patching access resistance were continuously monitored during the
320 experiment and cells which exhibited more than 15–20% changes in these parameters
321 were excluded from analysis.

322 In order to preserve a relatively intact neuronal circuit, no receptor antagonists were
323 used. Spontaneous excitatory post-synaptic currents (sEPSCs) were collected at a
324 membrane holding potential of -70 mV, which is close to the calculated reverse potential
325 of GABA. In order to measure the excitatory and inhibitory input on the same neuron,
326 the spontaneous inhibitory post-synaptic currents (sIPSCs) were also measured on the
327 same neuron but this time the holding potential was increased to 5-10 mV, a potential
328 close to the reverse potential of excitatory input, without visual negative deflection.
329 Recorded neuronal activities were detected as described previously (Lillis et al., 2015)
330 by custom software (DClamp: available at www.ieeg.org/?q=node/34). Integrated
331 excitatory conductance (sEPSCs, G_E) and integrated inhibitory conductance (sIPSCs,

332 G_I) were calculated as previously reported $G_E = \int_0^t \frac{sEPSCs}{t(V_M - V_{Erev})}$ and $G_I = \int_0^t \frac{sIPSCs}{t(V_M - V_{Irev})}$

333 (Slomowitz et al., 2015).

334 **Preparation of mouse brain homogenates and detection of APP**

335 Certain brain slices from wild-type and APP knock-out mice were frozen immediately
336 after completion of electrophysiological recording (Figures 4, 5 and 6) and stored at -
337 80°C until analyzed. Tissue (~0.1 mg) was homogenized in 5 volumes (w/v) of ice-cold
338 20 mM Tris-HCl, containing 150 mM NaCl and 1%TX-100 (TBS-Tx), pH 7.4 containing
339 protease inhibitors and centrifuged at 100,000 g and 4°C for 78 minutes in a TLA-55
340 rotor (Beckman Coulter, Fullerton, CA). The upper 90% of the supernatant was
341 removed, aliquoted and stored at -80°C pending analysis. Ten µg of total protein was
342 boiled in 1 x sample buffer (62.5 mM Tris, 1% w/v SDS, 10% v/v glycerol, 0.01% phenol
343 red and 2% β-mercaptoethanol) for 5 minutes and electrophoresed on hand poured, 15
344 well 10% polyacrylamide tris-glycine gels. Gels were rinsed in transfer buffer (10%
345 methanol, 192 mM Glycine and 25 mM Tris) and proteins electroblotted onto 0.2 µM
346 nitrocellulose membranes at 400 mA and 4°C for 2.5 hours. Membranes were
347 developed using the anti-APP antibody, 22C11, and bands visualized using a Li-COR
348 Odyssey infrared imaging system (Li-COR, Lincoln, NE).

349

350 **Array tomography (AT) imaging of mouse brain slices**

351 Upon completion of electrophysiology recordings certain brain slices from wild-type and
352 APP knock mice (Figures 4, 5 and 6) were processed for array tomography (Koffie et al.,
353 2009; Pickett et al., 2016). Slices were fixed in PBS containing 4% paraformaldehyde
354 and 2.5% sucrose at 4°C overnight. Samples were then washed three times (10

355 minutes each) in cold wash buffer (PBS containing 3.5% sucrose and 50 mM glycine),
356 and the hippocampus dissected out under a Leica Wild M3Z Stereozoom Microscope
357 (Heerbrugg, Switzerland). Thereafter hippocampi were dehydrated using an ethanol
358 gradient of: 50%, 70%, 95% and 100%. Tissue was then placed into a solution of 1:1
359 ethanol: LR White resin (Electron Microscopy Sciences) for 5minute and then washed 3
360 times with LR White. Tissue was incubated overnight at 4°C in LR White, embedded in
361 a gelatin capsule and polymerized overnight at 53°C. Three embedded blocks per
362 condition were cut into ribbons of 70 nm sections on an ultracut microtome (Leica) using
363 a Jumbo Histo Diamond Knife (Diatome). Ribbons were collected on gelatin-coated
364 glass coverslips, stained with antibodies and imaged along the ribbon. Two ribbons per
365 slice were collected and one was stained for PSD95 and 1C22 and the other for
366 synapsin-1 and 1C22. Primary antibodies were 1C22 (1:50), rabbit anti-PSD95 (3450P,
367 Cell Signaling, at 1:50), and rabbit anti-synapsin-1 (AB1543P, Millipore, at 1:100).
368 Secondary antibodies donkey anti-mouse 488 (A21202) and donkey anti-rabbit 594
369 (A21207) were from Invitrogen and used at 1:50.

370 Two image stacks per ribbon were collected from the stratum radiatum using a Zeiss
371 axio Imager Z2 epifluorescent microscope with a 63X 1.4NA Plan Apochromat objective.
372 Images were acquired with a CoolSnap digital camera and AxioImager software with
373 array tomography macros (Carl Zeiss, Ltd, Cambridge UK). Images from each set of
374 serial sections were compiled to create a 3D stack and aligned using ImageJ
375 multistackreg macros (Kay et al., 2013). Regions of interest (10 μm x 10 μm) were
376 selected, cropped and thresholded in Image J (Schindelin et al., 2012; Ollion et al.,
377 2013) (Figure 1). Custom MATLAB macros were used to remove single slice punctuate,

378 count synaptic punctuate and assess co-localization with 1C22 (a minimum of 50%
379 overlap between 1C22 and synaptic punctuate was required to be designated as co-
380 localization). All custom analysis macros will be freely available on
381 <http://datashare.is.ed.ac.uk> after publication.

382

383 **Data analysis and Statistical test**

384 Figures showing IP/WB and MSD A β immunoassay data are representative of at least 2
385 independent experiments. For electrophysiological experiments, the AD, ID-AD and
386 aCSF samples were coded and tested in an interleaved manner to avoid variances in
387 animals or slice quality influencing results. Slices in each group came from different
388 animals unless otherwise noted. Electrophysiological data were analyzed offline by
389 pclamp 10.2 (Molecular Devices, Sunnyvale, CA) and tested with One-way or Two-way
390 analysis of variance (ANOVA) with Bonferroni *post-hoc* tests or student's *t*-tests (#
391 $p < 0.05$, ## $p < 0.01$, and ### $p < 0.001$). A Kolmogorov–Smirnov (K–S) test was used to
392 compute differences in distributions of sEPSCs and sIPSCs. Array tomography was
393 analyzed using SPSS Version 22. A single percent co-localization for each parameter
394 was calculated for each slice from approximately 41 regions of interest and $\approx 7,500$
395 synapses ($\sim 3,500$ pre-synapses and $\sim 3,500$ post-synapses) were analyzed per slice
396 and tested with a Kruskal-Wallis with Dunns *post-hoc* test. Electrophysiology data are
397 shown as means \pm SEM. Array tomography data is shown as medians \pm the
398 interquartile range, each point representing all synapses measured within 1 slice.

399 Analyses of the same sample using different slices are considered technical replicates
400 and analysis of extracts from different AD brains are considered biological replicates.

401

402 **Results**

403 We previously reported that aqueous extracts of certain end-stage AD brains block
404 hippocampal LTP *in vivo* and *in vitro* (Shankar et al., 2008; Barry et al., 2011; Freir et al.,
405 2011; Jo et al., 2014). Here we further investigated the mechanism of this effect and
406 the requirement of endogenous APP.

407

408 **The water-soluble extract from AD brain contains both A β monomers and** 409 **oligomers and blocks LTP in a manner dependent on A β**

410 Brain extracts were prepared as described and a portion was immunodepleted (ID) of
411 A β or mock-ID with pre-immune rabbit serum. Here, the mock-ID extract is referred to
412 as the AD sample, and the material depleted of A β as ID-AD. ID and AD samples from
413 AD1 were analyzed using IP/WB, and MSD immunoassays that preferentially recognize
414 either A β oligomers (oAssay) or A β 42 monomers (Mc Donald et al., 2015). IP/WB
415 analysis allows the capture of A β structures under native conditions and their detection
416 following denaturing SDS-PAGE. We were careful to also determine if AW7 altered
417 APP metabolites present in AD brain extracts that contained all or part of the A β
418 sequence i.e. APPs α , N-terminally extended A β (-31A β 40), or so-called A η peptides.
419 To this end AW7 IPs were used for Western blotting with (i) the C-terminal anti-A β
420 antibodies, 2G3 and 21F12, and (ii) the N-terminal anti-A β antibody, 6E10. The latter,
421 but not the former, reacts with APPs α and A η - α peptides (Portelius et al., 2013; Welzel
422 et al., 2014; Willem et al., 2015). 6E10 readily detected ~4 kDa A β , but it did not detect

423 any bands consistent with APPs α or A η - α . Furthermore, direct Western blot analysis of
424 AD brain extract demonstrated highly similar levels of APPs in both AW7 and mock
425 immunodepleted extracts. Thus, it appears that AW7 does not deplete AD extracts of
426 non-A β APP metabolites that contain the N-terminal portion of A β (Figure 2A). The ~7
427 kDa A β species detected with 2G3 and 21F12 was not detected with 6E10, consistent
428 with our prior observation that most ~7 kDa A β is N-terminally truncated - a pattern we
429 have seen in aqueous extracts of more than 100 AD brains analyzed in our laboratory
430 (Mc Donald et al., 2015). Since SDS-PAGE is highly denaturing, the ~4 and ~7 kDa
431 species do not necessarily reflect native A β species. Rather, these simply indicate that
432 at least two different A β species are present. The same samples were treated with or
433 without 5 M GuHCl and then analyzed using MSD assays. In prior studies we found
434 that GuHCl effectively disaggregates high molecular weight A β species such that the
435 signal detected by our oAssay is greatly decreased, whereas the signal detected by the
436 monomer-preferring A β x-42 immunoassay is proportionately increased (Mably et al.,
437 2015). A similar outcome was evident when the extract of AD1 was treated with GuHCl
438 (Figure 2B). Specifically, GuHCl treatment caused a ~70% decrease in the oligomer
439 signal and a more than 8-fold increase in the monomer signal. Together these
440 immunoassay and IP/WB results indicate that the majority of A β in the AD1 extract exist
441 as labile aggregates made up of ~4 kDa A β and ~7 kDa A β . Importantly, AW7 ID
442 effectively removed the large majority of the various A β species detected (Figure 2A
443 and B). For instance, AW7 ID reduced the oligomer signal from 5.1 ± 0.03 ng/ml to 0.32
444 ± 0.12 ng/ml (Figure 2B, left panel) and monomer from 3.42 ± 0.03 ng/ml to 0.12 ± 0.04
445 ng/ml (Figure 2B, right panel).

446 For slices that received vehicle aCSF-B (Control), TBS induced strong potentiation
447 which lasted the whole recording period (Figure 2C, black circles, $181.1 \pm 10.7 \%$, $n =$
448 17), and ID-AD1 allowed a similar response (green downward triangles, $173.6 \pm 8.7 \%$,
449 $n = 11$, $p=0.12$, One-Way ANOVA) (Figure 2C and D). Consistent with prior reports
450 (Shankar et al., 2008; Freir et al., 2011), application of the AD1 (magenta diamonds)
451 extract significantly decreased LTP compared to both the control and ID-AD1 treatment
452 ($136 \pm 4.2 \%$, $n = 18$, $F=4.26$, $p=6.98E-9$ AD1 vs. Control; $F=4.14$, $p=3.56E-12$ AD1 vs.
453 ID-AD1, One-Way ANOVA). The fact that the ID-AD1 and AD1 samples are identical
454 except that the latter contains more A β than the former, is evidence that some form of
455 A β is responsible for the block of LTP induced by the AD1 extract. To further test the
456 A β dependency of the block of LTP mediated by AD1, we examined whether an extract
457 from a non-AD brain (NC), could impair LTP. As anticipated, the NC extract lacked
458 appreciable levels of A β (not shown) and did not impair LTP (Figure 2E and F, $159.54 \pm$
459 10.6% in NC, $n = 8$; $160.36 \pm 6.26 \%$ in Control, $n = 8$; $F=4.6$, $p=0.95$ One-Way
460 ANOVA).

461

462 **A β -containing AD brain extract affects pre-synaptic release probabilities**

463 Accumulating evidence indicates that soluble A β species may interact with excitatory
464 and inhibitory pre-synaptic terminals, modulate neurotransmitter release and cause
465 synaptic dysfunction in the very early stages of AD (Nimmrich et al., 2008; Abramov et
466 al., 2009; Kabogo et al., 2010; Parodi et al., 2010; Russell et al., 2012; Sokolow et al.,
467 2012; Huang et al., 2013; Ripoli et al., 2013; Kurudenkandy et al., 2014). Although the

468 effects of A β on LTP are well established (Klyubin et al., 2012), little is known about
469 whether and how A β -containing AD extracts affect pre- and post-synaptic elements. To
470 investigate effects on pre-synaptic release, we measured short-term synaptic facilitation
471 (Zucker and Regehr, 2002) in slices before and 30 minutes after treatment with AD1
472 extract. As synapse release probability is inversely correlated to synaptic facilitation
473 (Zucker and Regehr, 2002), we employed high-frequency burst stimulation (5 pulses
474 with 20 millisecond intra-burst stimulus interval). Application of AD1 extract induced a
475 reduction in the short-term facilitation during burst stimulation (Figure 3A and B). When
476 responses were normalized based on the ratio of each fEPSP to the first response, we
477 found that treatment with AD1 extract had no effect on the 2nd response, but significantly
478 decreased the 3rd, 4th, and 5th response (magenta circles, $p=0.02$ at 3rd stimulation,
479 $p=0.004$ at 4th stimulation and $p=0.004$ at 5th stimulation, $n = 6$, student's t -test, and also
480 by group and time with Two-way ANOVA, $F_{(4,7)}=6.39$, $p=0.006$) (Figure 3B). In contrast,
481 the slices treated with ID-AD1 yielded a pattern highly similar to that obtained with
482 aCSF-B control ($n = 7$, $F=5.32$, $p=0.91$, Two-Way ANOVA, Figure 3C and D). Thus, A β
483 in the AD extract caused a reduction in short-term synaptic plasticity associated with
484 increased pre-synaptic glutamate release.

485

486 **A β -containing AD brain extract disrupts the excitation-to-inhibition balance**

487 To estimate the effect of A β on the total synaptic input at the single-neuron level, we
488 used whole-cell voltage clamp recordings to measure spontaneous excitatory
489 postsynaptic currents (sEPSCs) on CA1 pyramidal neurons before and 30 minutes after

490 addition of AD extract. The holding potential was kept constant at -70 mV and sEPSCs
491 measured before and 30 minutes after addition of AD1 extract – this 30 minutes interval
492 was chosen to match the pre-incubation time used in our LTP and short-term facilitation
493 experiments. Application of the AD1 extract significantly decreased the inter-event
494 interval ($p=1.65E-6$, K-S test) and increased the mean frequency of sEPSCs (from $1.8 \pm$
495 0.2 Hz to 2.7 ± 0.3 Hz, $p=0.02$, $n = 7$, student's t -test) (Figure 4A and B), but did not
496 alter the sEPSCs amplitude (mean amplitude from 11.7 ± 1.8 pA to 10.1 ± 1.6 pA,
497 $p=0.65$, $n = 7$, student's t -test) (Figure 4A and C). In contrast, the ID-AD1 sample had
498 no effect on the frequency or the amplitude of sEPSCs (mean frequency: from 2.2 ± 0.5
499 Hz to 2.3 ± 0.7 Hz, mean amplitude: from 9.7 ± 1.7 pA to 10.2 ± 1.4 pA, $p=0.45$, $n = 6$,
500 student's t -test) (Figure 4D–F). These results indicate that the AD brain-derived A β
501 significantly augments excitatory synaptic input on CA1 pyramidal neurons.

502 Pyramidal neurons receive both excitatory (sEPSCs) and inhibitory (sIPSCs) inputs,
503 GABAergic axon terminals more easily form synapses with perisomatic regions of
504 pyramidal cells and strongly influence the output of neurons (DeFelipe, 2002; Garcia-
505 Marin et al., 2009). To record sIPSCs on the same neurons, we adjusted the holding
506 potential to 5 mV, a voltage close to the calculated sEPSCs reverse potential. As
507 shown in Figure 4G–I, the AD1 sample significantly increased inter-event intervals
508 ($p=6.19E-6$, K-S test) and decreased the frequency of sIPSCs (from 4.7 ± 0.7 Hz to 3.1
509 ± 0.7 Hz, $p=0.008$, $n = 7$, student's t -test), without altering sIPSCs amplitude (from 14.8
510 ± 1.4 pA to 14.2 ± 0.9 pA, $p=0.75$, $n = 7$, student's t -test). In contrast, the ID-AD1
511 sample had no effect on sIPSCs (frequency: from 5.3 ± 0.4 Hz to 4.8 ± 0.7 Hz,
512 amplitude: from 13.6 ± 1.6 pA to 13.2 ± 2.1 pA, $p=0.21$, $n = 6$, student's t -test) (Figure

513 4J-L). These results revealed that brain-derived A β significantly reduces GABAergic
514 input on CA1 pyramidal cells.

515 To assess whether the changes of excitatory input (E) and inhibitory input (I) to the
516 same neuron affect the E/I balance of that neuron, we calculated the integrated
517 conductance of sEPSCs and sIPSCs over a 5 minutes period (Figure 4M). Comparison
518 of the integrated conductance before and 30 minutes after AD1 sample application
519 revealed E was increased ~3 fold and I was decreased ~50%, consequently, the E/I
520 balance was increased ~6 fold ($n = 7$) (Figure 4N). These results show that AD brain-
521 derived A β oppositely affects excitatory and inhibitory synaptic transmission, causing an
522 increase in the E/I ratio. These changes, especially the reduction of GABAergic tone on
523 individual neurons, may contribute to neuronal hyperactivity and disturb network
524 homeostasis, thereby perturbing LTP (Wang et al., 2014; Gillespie et al., 2016).

525
526 **Genetic ablation of APP occludes the effects of A β on LTP and pre-synaptic**
527 **activity and normalizes the E/I balance**

528 Multiple lines of evidence suggest that the APP may play a role in both GABAergic and
529 glutamatergic neurotransmission (Bai et al., 2008; Kabogo et al., 2010; Pliassova et al.,
530 2016; Schwenk et al., 2016) and separate studies impute a link between A β and APP
531 (Lorenzo et al., 2000; Fogel et al., 2014; Kirouac et al., 2017). Thus, having found that
532 brain-derived A β acts on pre-synapses and modulates both GABA and glutamate
533 transmission, we investigated if APP was required for these effects. For this, we
534 employed mice null for APP (Figure 5A). In agreement with prior reports, brain slices

535 from APP KO and WT littermate mice exhibited similar levels of basal activity ($p=0.19$,
536 One-Way ANOVA) and LTP (Figure 5B and C) (Dawson et al., 1999; Jedlicka et al.,
537 2012). In both WT and APP KO slices treated with the aCSF-B control, TBS induced
538 strong potentiation which lasted the whole recording period (158.1 ± 6.3 % in WT, $n =$
539 11, black circles; 151.2 ± 8.5 % in APP KO, $n = 9$, gray hexagons; $F=4.4$, $p=0.79$,
540 comparison of the last 10 minutes of recording using One-Way ANOVA) (Figure 5C and
541 D). In agreement with experiments shown in Figure 2, addition of AD1 extract to WT
542 slices significantly decreased LTP compared to addition of aCSF-B (121.8 ± 5.4 % in
543 WT + AD1, magenta diamonds, $n = 7$, $F=4.5$, $p=0.0005$, WT Ctr vs. WT + AD1, One-
544 Way ANOVA). However, application of the same extract to slices from APP KO mice
545 had no effect on LTP, with the level of LTP in APP KOs indistinguishable from that of
546 WT or APP KO treated with aCSF-B control (145.4 ± 4.2 % in APP KO + AD1, pink
547 upward triangles, $F=4.5$, $p=0.41$, APP KO Ctr vs. APP KO + AD1; One-Way ANOVA).
548 Similarly, when applied to APP KO brain slices, AD1 extract had no effect on short-term
549 facilitation (Figure 5E and F).

550 To assess the generalizability of the rescue of LTP by APP ablation, we tested the
551 effect of an extract from a second AD brain (AD2) on another APP KO mouse line
552 (Zheng et al., 1995). As with the AD1 extract (Figure 2), the AD2 and ID-AD2 extracts
553 were characterized by IP/WB and ELISA. The profiles obtained for AD2 (Figure 6A)
554 were similar to those of AD1 (Figure 2A), except AD2 contained relatively more ~7 kDa
555 species than AD1 (Figure 6 A and B). As seen with the first APP KO line tested (Figure
556 5), brain slices from the second APP KO line (which we refer to as Zheng APP KOs)
557 (Zheng et al., 1995) exhibited similar levels of basal activity as slices from wild type

558 mice ($F=4.6$, $p=0.91$, One-Way ANOVA) (Figure 6E and F). When AD2 extract was
559 applied to slices from WT mice it blocked LTP in an $A\beta$ -dependent fashion (184.1 ± 7.7 %
560 in WT Ctr, black circles, $n = 12$; 137.1 ± 7.2 % in WT + AD2, magenta diamonds, $n = 12$;
561 $F=4.96$, $p=0.0001$, One-Way ANOVA), but had no effect on LTP elicited from APP KO
562 mice (175.8 ± 9 % in APP KO Ctr, gray hexagons, $n = 11$; 169.9 ± 4 % in APP KO +
563 AD2, pink upward triangles, $n = 12$; $F=5.12$, $p=0.56$, One-Way ANOVA) (Figure 7A and
564 B).

565 To further examine whether the APP-dependent block of LTP by AD brain extracts was
566 indeed mediated by $A\beta$ and not some other AW7-reactive material, we tested if the well-
567 established block of LTP mediated by ADDLs (Lambert et al., 1998; Wang et al., 2002;
568 Lauren et al., 2009; Freir et al., 2011) also required expression of APP. ADDLs were
569 prepared as described previously and then assessed using SEC and EM (Figure 6C
570 and D). The ADDL preparation contained a mixture of $A\beta$ aggregates and a small
571 amount of monomer (Figure 6C and D). When applied to brain slices from WT mice,
572 ADDLs (200 nM) blocked LTP (188.9 ± 11.5 % in WT Ctr, black circles, $n = 8$; 123.8 ± 6 %
573 in WT + ADDLs, magenta diamonds, $n = 6$; $F=4.75$, $p=0.0007$, One-Way ANOVA), but
574 had no effect on LTP elicited from APP KO slices (181.5 ± 15 % in APP KO Ctr, gray
575 hexagons, $n = 7$; 168.1 ± 10 % in APP KO + ADDLs, pink upward triangles, $n = 7$;
576 $F=4.85$, $p=0.07$, One-Way ANOVA) (Figure 7C and D). Thus, it appears that the well-
577 documented plasticity-disrupting activity of both $A\beta$ extracted from AD brains (Klyubin et
578 al., 2008; Shankar et al., 2008; Barry et al., 2011; Freir et al., 2011; Klyubin et al., 2012)

579 and synthetic A β (Lambert et al., 1998; Wang et al., 2002; Lauren et al., 2009; Freir et
580 al., 2011) require expression of APP.

581 To investigate whether APP is necessary for the effect of A β on the E/I balance (Figure
582 3), we studied the effects of A β on sEPSCs and sIPSCs in brains of Zheng APP KO and
583 WT littermate mice (Figure 8). When applied to WT slices, AD1 extract again increased
584 mean sEPSC frequency (from 2.2 ± 0.1 Hz to 3.4 ± 0.2 Hz, $p=0.003$, $n = 5$, student's t -
585 test) and decreased inter-event intervals ($p=6.34E-15$, K-S test), without altering the
586 amplitude of sEPSCs (mean amplitude: 17.8 ± 0.4 pA vs. 18 ± 1.5 pA, $p=0.32$, $n = 5$,
587 student's t -test) (Figure 8A-C); and on the same neuron decreased mean sIPSCs
588 frequency (from 4.2 ± 0.8 Hz to 2.7 ± 0.4 Hz, $p=0.006$, $n = 5$, student's t -test) and
589 increased inter-event intervals ($p=9.44E-20$, K-S test), but not amplitude (mean
590 amplitude from 20 ± 3 pA to 19.3 ± 1.3 pA, $p=0.34$, $n = 5$, student's t -test) (Figure 8D-F).
591 These results, which were obtained with WT mice from an entirely different colony as
592 those used in Figure 2, nicely demonstrate the robustness of the A β effect (See Figure
593 4 vs. Figure 8). Most importantly, when AD1 extract was applied to Zheng APP KO
594 slices there was no change in the frequency or amplitude of sEPSCs (mean frequency:
595 from 2.6 ± 0.1 Hz to 2.7 ± 0.4 Hz, mean amplitude: from 15 ± 1.4 pA to 14.6 ± 0.5 pA,
596 $p=0.14$, K-S test; $p=0.26$, $n = 6$, student's t -test) (Figure 8G-I). Similarly, sIPSCs were
597 also unchanged (mean frequency: from 3.5 ± 0.5 Hz to 3.5 ± 0.3 Hz, mean amplitude:
598 from 16.7 ± 1 pA to 16.4 ± 1.6 pA, $p=0.58$, K-S test; $p=0.25$, $n = 6$, student's t -test
599 (Figure 8J-L). Thus, as with our LTP experiments (Figures 5 and 7), ablation of APP
600 completely rescued the effects of A β on excitatory and inhibitory input on CA1 pyramidal
601 neurons. Further, since APP KO occluded A β alterations on the E and I input at

602 individual neurons, it also prevented A β -mediated changes in the integrated
603 conductance of sEPSCs and sIPSCs (Figure 8M). When AD1 extract was applied to
604 WT slices, E increased ~3-fold and I decreased ~44%, resulting in ~5.8-fold increase in
605 the E/I ratio. However, APP KO significantly prevented those E/I ratio changes
606 ($p=0.001$, E/I in WT vs. E/I in APP KO, One-Way ANOVA) (Figure 8M). These results
607 indicate that APP plays an important role in regulating the acute effects of A β on
608 excitatory and inhibitory pre-synaptic release, and consequent maintenance of network
609 homeostasis.

610

611 **A β binding to synapses requires APP**

612 To further investigate the targeting of synaptic elements by A β and how this might be
613 influenced by APP we used a powerful high-resolution microscopic technique, array
614 tomography (AT), to search for evidence of A β binding to synapses in the same brain
615 slices used in our electrophysiology experiments. Upon completion of LTP recording,
616 certain slices from the treatment groups used in Figures 2C and 5C were immediately
617 fixed, processed and used for AT. Sections were stained with 1C22 – the same
618 aggregate-preferring antibody (Mably et al., 2015; Pickett et al., 2016) used in our
619 oAssay, anti-synapsin-1 (for pre-synapses) and anti-PSD95 (for post-synapses).
620 Approximately 7,000 synapses (~3,500 pre-synapses and ~3,500 post-synapses) per
621 slice were analyzed for a total of 100,359 pre-synapses and 99,075 post-synapses. AT
622 revealed, significant anti-A β staining at synapse of slices incubated with AD1 extract,
623 with only background staining in samples incubated with aCSF controls and ID-AD1

624 (Figure 9A-C; Kruskal Wallis test for synapsin-1 ($\chi^2_{(4)}=10.844$, $p=0.028$), Kruskal Wallis
625 test for PSD95 ($\chi^2_{(4)}=11.583$, $p=0.021$)). In slices incubated with AD1 extract $1.27 \pm$
626 0.47% of pre-synapses and $0.58 \pm 0.19\%$ of post-synapses stained with 1C22, whereas
627 in slices that had been incubated with aCSF, only $0.0076 \pm 0.013\%$ of pre-synapses
628 and $0.0184 \pm 0.087\%$ of post-synapses were 1C22 positive (Dunns *post-hoc* between
629 AD and control for pre-synapses $p=0.024$ and for post-synapses $p=0.010$). Slices
630 incubated with extracts immunodepleted of A β exhibited similar background staining
631 with 1C22 as the aCSF control (Figure 9A-C). Thus, the same treatment with AD1
632 extract that disrupts synaptic plasticity in an A β -dependent fashion (Figures 2 and 4)
633 also leads to A β binding to synapses (Figure 9A-C). Moreover, the finding that A β is
634 present at more pre-synapses than post-synapses (Mann-Whitney U between AD pre-
635 synapses and AD post-synapses $U=0$, $p=0.004$) is consistent with our results that
636 suggest a pre-synaptic effect of A β (Figures 4 and 8), and with preliminary experiments
637 using an antibody to another pre-synaptic marker, synaptophysin.

638 The number of A β positive synapses detected here is much lower than the amount of
639 A β observed at synapses when synthetic oligomers are applied to cultured hippocampal
640 neurons (Lacor et al., 2004; Lacor et al., 2007). However, the current paradigm, of
641 applying soluble AD brain extract to intact mouse brain slices is more relevant to the *in*
642 *vivo* situation than model systems in which A β is applied directly and at high
643 concentrations to dissociated neurons (Lacor et al., 2004; Lacor et al., 2007). Indeed, it
644 is noteworthy that the percentage of synapses positive for A β in the current study are
645 consistent with our findings in APP transgenic mouse brain where we observed
646 approximately 1% of postsynaptic densities (PSDs) positive for A β distant from plaques

647 (Koffie et al., 2009). Similarly, in human AD brain at sites distant from plaques, we
648 detected A β at 0.6% of PSDs and 0.5% of pre-synaptic terminals (Koffie et al., 2012).
649 Thus, at disease relevant concentrations sufficient to disrupt plasticity, synaptic A β
650 binding occurs at levels similar to that observed in human AD brain.

651 Importantly, when brain slices from APP KO mice were incubated with AD1 extract, little
652 or no synaptic 1C22 staining was detected (Figure 9A-C). These results are notable
653 since expression of APP was found to be required for A β -mediated disruption of both
654 long-term plasticity (Figures 5 and 7) and neurotransmitter release (Figure 8). In sum,
655 our AT data are completely congruent with the results of our electrophysiological
656 experiments and indicate that expression of APP is required for the binding and
657 subsequent plasticity-disrupting effects of A β , and that these effects are largely
658 mediated on the pre-synapse.

659

660 **APP mediates binding of synaptotoxic A β to brain cells**

661 We reasoned that if synaptotoxic forms of A β bound to APP or to an APP containing
662 complex then it should be possible to pre-treat bioactive extracts with a source of APP
663 to deplete the extract of activity. One possible approach would be to add exogenous
664 recombinant APP, but APP is a transmembrane protein and its expression outside of a
665 membrane environment in the absence of proper post-translational modifications
666 precludes its use. Instead, we pre-incubated AD2 extract with either APP-containing
667 (WT) or APP lacking (KO) brain slices (Figure 10A). When AD2 was pre-incubated with

668 WT brain slices and then applied to a fresh WT brain slice it was no longer capable of
669 blocking LTP (216.4 ± 26 % in WT slices + AD2, green upward triangles, $n = 6$; $F=4.96$,
670 $p=0.82$, One-Way ANOVA) (Figure 10B and C). In contrast, when AD2 extract was pre-
671 incubated with APP KO slices and then applied to a fresh WT brain slice, the AD2
672 extract retained its ability to block LTP (210.3 ± 15 % in WT Ctr, black circles, $n = 6$;
673 146.8 ± 5.4 % in APP KO +AD2, magenta diamonds, $n = 6$; $F=4.96$, $p=0.003$, One-Way
674 ANOVA, Figure 10B and C). These results are entirely consistent with our array
675 tomography experiments and provide further evidence that APP enables synaptotoxic
676 forms of A β to bind to and perturb neurons.

677

678 **A β -containing AD brain extract partially blocks LTP in APP hemizygous brain** 679 **slices**

680 To further investigate the requirement of APP for A β synaptotoxicity, we tested the
681 effect of AD2 extract on brain slices from APP hemizygous mice. APP expressing wild
682 type C57BL/6 were bred with Zheng APP KO mice and the hemizygous progeny used
683 for LTP experiments. Hemizygous mice express 50% as much APP as WT mice
684 (Figure 11A) and exhibit similar levels of basal activity relative to slices from wild type
685 mice ($F=4.6$, $p=0.75$, One-Way ANOVA) (Figure 11B). The control level of LTP was
686 also similar in WT and hemizygous brain slices (187.85 ± 5.63 % in WT Ctr, black
687 circles, $n = 9$; 189.69 ± 7.19 % in hemizygous brain slices, gray hexagons, $n = 9$;
688 $F=4.45$, $p=0.84$, One-Way ANOVA) (Figure 11C and D). When AD2 extract was
689 applied to slices from WT mice it blocked LTP to an extent comparable to that seen in

690 previous experiments (compare Figure 11C and D versus Figure 7A and B) ($187.85 \pm$
691 5.63 % in WT Ctr, black circles, $n = 9$; 136.93 ± 3.14 % in WT + AD2, magenta
692 diamonds, $n = 10$; $F=4.5$, $p=2.67E-007$, One-Way ANOVA). Similarly, AD2 extract
693 impaired LTP in APP hemizygous mice (189.69 ± 7.19 % in APP +/- Ctr, gray hexagons,
694 $n = 9$; 154.83 ± 6 % in APP +/- AD2, pink upward triangles, $n = 10$; $F=4.49$, $p=0.003$,
695 One-Way ANOVA) (Figure 11C and D). Although the extent of the block in hemizygous
696 slices was somewhat reduced compared WT slices ($F=4.45$, $p=0.84$, Control in WT
697 mice vs. Control in APP +/- mice; $F=4.5$, $p=2.67E-007$, Control vs. AD2 in WT mice;
698 $F=4.49$, $p=0.003$, Control vs. AD2 in WT mice; One-Way ANOVA), the effect of AD2
699 extract on hemizygous brain slices stands in contrast to its lack of effect on APP KO
700 slices (Figure 7A and B). The partial attenuation of $A\beta$ synaptotoxicity in APP
701 hemizygous brain indicates a gene-dose effect, such that 50% of the normal level of
702 APP is sufficient to mediate some block of LTP, but not the full block of LTP seen in
703 APP WT mice. Further studies will be required to determine the minimal reduction in
704 APP levels that allows full protection against the plasticity disrupting effects of $A\beta$.

705

706 **Discussion**

707 To better understand how A β disrupts synaptic plasticity we combined the use of the
708 most disease relevant form of A β , material extracted from human AD brain, with
709 electrophysiological approaches and high-resolution microscopy. Consistent with prior
710 studies, we show that extracts from the brains of individuals who died with AD block
711 LTP (Shankar et al., 2008; Barry et al., 2011; Freir et al., 2011; Yang et al., 2017). We
712 further show that, concomitant with the block of LTP, there is an increase in pre-
713 synaptic release and disruption of E/I balance. In accord with these synaptic effects of
714 A β , we demonstrate that exogenously applied AD brain-derived A β binds to synapses,
715 with more A β oligomers detected on pre-synapses than on the post-synapses. Our
716 finding that treatment with brain-derived A β enhances excitatory drive agrees well with
717 studies showing that aggregated forms of synthetic A β increase EPSPs, action
718 potentials, and membrane depolarizations (Hartley et al., 1999; Minkeviciene et al.,
719 2009; Kurudenkandy et al., 2014). Our study is unique in that we employed brain-
720 derived A β , and that the concentration of this material was much lower than the
721 synthetic A β used in prior studies. In support of the strength of this experimental
722 paradigm, the levels of synaptic A β we observe in this study are very similar to those
723 observed with array tomography in our studies of human AD brain (Koffie et al., 2012).
724 The apparent paradox that ectopic application of A β causes a net increase in excitation,
725 yet impairs LTP may result because of glutamate spillover and activation of extra- or
726 perisynaptic NR2B-enriched NMDARs, which play a major role in LTD induction (Li et
727 al., 2011; Zhang et al., 2016). In such a scenario, synaptic depression may result from
728 an initial increase in synaptic activation of NMDARs by glutamate, followed by synaptic

729 NMDAR desensitization, NMDAR/AMPA internalization, and activation of
730 extrasynaptic NMDARs and mGluRs (Born et al., 2014). However, it is unclear why
731 ablation of APP could recover such effects.

732 An alternative explanation that accounts for a role for APP in the impairment of post-
733 synaptic efficacy is that exogenous AD brain-derived soluble aggregates and
734 endogenously produced monomer have differential effects. A β is known to be released
735 in an activity-dependent manner (Kamenetz et al., 2003; Cirrito et al., 2005), whereas
736 elevated A β levels result in depressed glutamatergic synaptic transmission and
737 glutamate receptor endocytosis (Kamenetz et al., 2003; Hsieh et al., 2006). Thus, it is
738 plausible that the increase in glutamate release induced by soluble A β aggregates may
739 also lead to an increase in *de novo* A β monomer production and this in turn may
740 depress post-synaptic activity. Such a scenario would necessarily require expression of
741 endogenous APP and explain why ablation of APP can obviate the block of LTP caused
742 by brain-derived soluble A β aggregates. The fact that A β treated APP hemizygous
743 slices exhibited an attenuated block is consistent with a partial reduction in the amount
744 of endogenous A β . With regard to the protection of LTP upon ablation of APP, it is
745 important to emphasize the robust nature and generalizability of this phenomenon. We
746 observed the same protection using two different APP KO mouse lines (Zheng et al.,
747 1995; Callahan et al., 2017), extracts from 2 different AD brains, and synthetic A β
748 oligomers. Both AD extracts blocked LTP in an A β -dependent manner when applied to
749 wild type mouse brain slices, but the same AD extracts had no effect on LTP elicited
750 from APP KO slices. Moreover, the extent of A β binding to synapses was similar in two

751 different sources of wild type mice (Figure 7B and C), and the pattern observed was
752 reminiscent of that seen in AD brain (Pickett et al., 2016).

753 There is evidence that APP can act as a receptor for A β (Melchor and Van Nostrand,
754 2000; Van Nostrand et al., 2002; Yankner and Lu, 2009; Fogel et al., 2014; Kirouac et
755 al., 2017) and that APP may mediate increased excitatory drive (Fogel et al., 2014).
756 Specifically, A β was unable to promote aberrant neurotransmitter release in the
757 absence of APP (Fogel et al., 2014). Our findings that binding of soluble A β aggregates
758 to synapses requires expression of APP and that synaptotoxic A β can be bound by APP
759 expressing, but not APP lacking brain tissue, are consistent, but not proof, that APP
760 may act as a receptor for A β . In this regard, it is worth noting that APP is known to both
761 regulate L-type calcium channels in GABAergic neurons, interact with the pore-forming
762 subunit Cav1.2 (Yang et al., 2009), and is a member of the GABA_B-R receptor complex
763 (Schwenk et al., 2016). In addition, there is evidence from proteomic studies indicating
764 that APP interacts with more than 30 different proteins including proteins key to synaptic
765 vesicle turnover (Kohli et al., 2012; Del Prete et al., 2014; Lassek et al., 2014; Wilhelm
766 et al., 2014), and proteins (such as the prion protein) implicated in binding A β (Bai et al.,
767 2008; Lauren et al., 2009). Thus, A β could exert an APP-dependent effect either by
768 directly binding to APP or binding to protein complexes of which APP is a component
769 and stabilizing member. The APP gene-dose dependent response to A β that we
770 observed is equally compatible with direct or indirect binding to APP.

771 So far we have considered the effects of A β on synapses and a single hippocampal
772 pathway (the *Schaffer Collateral*), but A β is also thought to have network-wide effects
773 (Palop and Mucke, 2010). For instance, A β -induced increases in excitatory network

774 activity could lead to synaptic depression through homeostatic mechanisms. It is well
775 established that acute treatment of primary neurons with bicuculline (a GABA_A
776 antagonist) increases overall neuronal activity and firing rates (Vertkin et al., 2015).
777 However, after a few days, neuronal activity returns to control levels. By analogy, it is
778 reasonable that the disruption of E/I balance seen with our acute A β treatment may also
779 cause both short-term local and long-lasting network effects. Given the fact that A β
780 treatment increases excitatory drive and decreases inhibitory drive, and that GABA-
781 ergic interneurons express high levels of APP in DG (Wang et al., 2014; Del Turco et al.,
782 2016) it is tempting to speculate that A β -mediated disruption of GABA-ergic
783 interneurons may play a critical role in the cognitive impairment that occurs early in AD
784 (Gillespie et al., 2016). Clearly, further studies will be required to delineate the influence
785 of APP on both network regulation and other forms of synaptic plasticity, such as LTD.
786 Considerable data from the study of APP transgenics implicate impairment of
787 GABAergic interneurons as central to the network disturbances evident in these models
788 (Busche and Konnerth, 2015; Palop and Mucke, 2016). However, the unphysiological
789 expression of high levels of APP and the concomitant release of A β from the expressed
790 transgene make it difficult to differentiate between effects mediated by A β versus APP,
791 or non-A β APP metabolites (Melnikova et al., 2013; Born et al., 2014; Fowler et al.,
792 2014). Nonetheless, growing evidence suggests that GABAergic interneurons play a
793 prominent role in homeostatic regulation of hippocampal networks, and there is
794 compelling proteomic and physiological data that link APP and GABA_{B1a}-R (Wang et al.,
795 2014; Gillespie et al., 2016; Schwenk et al., 2016). Consequently, further investigations
796 on how A β effects GABA_B-R expression, GABA_B-R-APP interactions and whether

797 GABA_B-R KO mice are resistant to A β and may lead to a pharmacological
798 means to attenuate A β synaptotoxicity. Similarly, modulation of APP expression may
799 also offer therapeutic potential. However, while our results demonstrate that ablation of
800 APP in brain slices from young (2-3 months) mice protects against the acute
801 synaptotoxicity of A β , widespread knock-out of APP is not recommended. APP appears
802 to be involved in many physiological processes (Yang et al., 2009; Muller and Zheng,
803 2012; Del Prete et al., 2014; Lassek et al., 2014; Wang et al., 2014) and aged APP null
804 mice exhibit hypersensitivity to kainate-induced seizures (Steinbach et al., 1998),
805 altered exploratory behavior, deficits in spatial memory, and impairment of LTP
806 (Dawson et al., 1999; Seabrook et al., 1999; Ring et al., 2007). No such deficits have
807 been reported in APP hemizygous mice. Thus, it may be possible to down regulate APP
808 expression so as to maintain normal function, yet attenuate A β synaptotoxicity.
809 However, hemizygous reduction of APP allows only partial protection against the
810 plasticity disrupting effects of A β , and further studies will be required to determine the
811 minimal reduction in APP levels that allows a more fulsome protection.

812

813 **Figure Legends**

814

815 **Figure 1. Processing of array tomography images.**

816 Fields of 10 μm by 10 μm are cropped from an image stack, these are then made into
817 binary stacks in image J and processed in MATLAB to remove objects not found in
818 serial slices. Scale bar is 2 μm .

819 **Figure 2. The water-soluble extract of AD brain, but not normal control,**
820 **contains both A β monomers and oligomers and perturbs long-term synaptic**
821 **plasticity.**

822 **(A)** Aqueous extract of AD1 was treated with either pre-immune rabbit serum or with
823 AW7 antiserum. Portions of the mock immunodepleted sample (AD1, magenta) and the
824 AW7 immunodepleted sample (ID-AD1, green) were then analyzed by IP/WB, using
825 AW7 for IP and a combination of 2G3 and 21F12 (left panel), or 6E10 (right panel) for
826 WB. **M** denotes A β monomer and * indicates a broad smear ~7–8 kDa. Synthetic A β 1-
827 42, -31A β 40 and A η - α each at 2 ng/lane were used as controls. As expected 6E10
828 detected all 3 synthetic peptides, whereas 2G3/21F12 detected A β 1-42, -31A β 40 but
829 not A η - α . Only non-specific (NS) bands were detected above 16kDa marker. **(B)** AD1
830 (magenta) and ID-AD1 (green) samples were incubated +/- 5 M GuHCl and analyzed
831 using immunoassays that preferentially recognize A β oligomers (1C22-3D6b, left panel)
832 or A β 42 monomer (266-21F12b, right panel). Values shown are the mean \pm SEM of
833 duplicate measurements and are representative of 2 separate experiments. **(C)** Time
834 course plots show that the AD sample but not the ID-AD sample blocked hippocampal
835 LTP. The gray horizontal bar indicates the time period when sample was present in the
836 bath. 1, 2, indicate example traces from time points just prior to the theta burst
837 stimulation ($\uparrow\uparrow\uparrow$ TBS) (1) and 60 minutes after TBS (2), respectively. The aCSF control
838 is shown in black circles; AD treatment is shown in magenta diamonds and ID-AD with
839 green downward triangles. Each slice used for each treatment was from a different
840 animal. Scale bar 0.2 mV, 10 milliseconds. **(D)** Histogram plots of the average

841 potentiation for the last 10 minutes of traces shown in **C**. Treatment of slices with AD1
842 sample significantly inhibited LTP compared to the aCSF vehicle control ($F=4.26$,
843 $p=6.98E-9$) and ID-AD1 treatment ($F=4.14$, $p=3.56E-12$); in contrast ID-AD1 had no
844 effect on LTP relative to the vehicle control ($F=4.23$, $p=0.12$, One-Way ANOVA).
845 Symbols are the same as in panel **C**. **(E)** Time course plots show that the brain extract
846 from a cognitively intact non-AD control (NC) did not blocked hippocampal LTP. The
847 gray horizontal bar indicates the time period when sample was present in the bath. 1, 2,
848 indicate example traces from time points just prior to the theta burst stimulation ($\uparrow\uparrow\uparrow$
849 TBS) (1) and 60 minutes after TBS (2), respectively. The aCSF control is shown in
850 black circles; NC treatment is shown in gray hexagons. Each slice used for each
851 treatment was from a different animal. Scale bar 0.5 mV, 10 milliseconds. **(F)**
852 Histogram plots of the average potentiation for the last 10 minutes of traces shown in **E**
853 and average of last 10 minutes from individual experiment in every group. Treatment of
854 slices with NC sample did not inhibited LTP compared to the aCSF vehicle control
855 ($F=4.6$, $p=0.95$, One-Way ANOVA). Symbols are the same as in panel **E**. Values
856 shown are the mean \pm SEM. ### $p<0.001$

857

858 **Figure 3. The A β -containing water-soluble extract of AD1 perturbs short-term**
859 **facilitation.**

860 **(A)** Representative traces of averaged field recordings were collected after 5 stimulation
861 bursts (inter-stimulation interval 20 milliseconds, inter-burst interval 30 seconds) before
862 (black, aCSF) and 30 minutes after perfusion with the AD1 sample (magenta). The trace
863 shown for the AD1 samples are scaled so that the first response matches that of the
864 aCSF control. Scale bars: 0.5 mV, 10 milliseconds. **(B)** fEPSPs amplitude after 2 to 5
865 stimulations were normalized to the value obtained after the first stimulation. Compared
866 to vehicle control, AD1 treatment induced a small but significant decrease in short-term
867 synaptic facilitation, ($p=0.02$) after the 3rd, ($p=0.004$) the 4th stimulation and 5th
868 stimulation ($p=0.004$); $n = 6$, student's t -test. Values shown are the mean \pm SEM. # $p <$
869 0.05 ; ## $p < 0.01$. **(C)** Representative traces of averaged field recordings were collected
870 after 5 stimulation bursts (inter-stimulation interval 20 milliseconds, inter-burst interval
871 30 seconds) before (black, aCSF) and 30 minutes after perfusion with the ID-AD1
872 sample (green). Scale bars: 0.4 mV, 10 milliseconds. ID-AD1 treatment did not affect
873 short-term synaptic facilitation ($n = 5$, $F=5.32$, $p=0.91$, One-Way ANOVA).

874 **Figure 4. AD brain-derived A β affects both excitatory and inhibitory synaptic**
875 **inputs, causing disruption of the excitatory/inhibitory ratio at individual CA1**
876 **neurons.**

877 **(A, D)** Example traces of spontaneous excitatory post-synaptic currents (sEPSCs)
878 before (aCSF, black) and 30 minutes after addition of sample (AD1, magenta; ID-AD1,
879 green) recorded from individual pyramidal neurons in the hippocampal CA1 area of
880 brain slices with the holding potential fixed at -70 mV. Scale bars: 20 pA, 700
881 millisecond. **(B)** 30 minutes of AD1 treatment decreased cumulative distributions of
882 inter-event intervals and increased mean frequency (insert) ($p=1.65E-6$, K-S test; $p<$
883 0.02 , student's t -test; $n = 7$), but **(C)** did not change the cumulative distributions or the
884 mean value (insert) of the amplitude of sEPSCs ($n = 7$). **(E, F)** The ID-AD1 sample had
885 no effect on either frequency or amplitude of sEPSCs ($n = 6$). **(G, J)** Example traces of
886 spontaneous inhibitory post-synaptic currents (sIPSCs) before (aCSF, black) and 30
887 minutes after treatment (AD1, magenta; ID-AD1, green) were recorded on the same
888 individual pyramidal neurons upon increasing the holding potential to 5 mV. Scale bars:
889 20 pA, 700 milliseconds. **(H)** 30 minutes of treatment with the AD1 sample increased
890 inter-event intervals and decreased mean frequency (insert) of sIPSCs (magenta)
891 versus aCSF (black) ($p=6.19E-6$, K-S test; $p=0.008$, student's t -test; $n = 7$). **(I)**
892 Treatment with the AD1 sample did not affect the amplitude of sIPSCs ($n = 7$) and the
893 ID-AD1 sample had no effect on frequency **(K)** or the amplitude **(L)** of sIPSCs versus
894 aCSF control ($n = 7$). **(M)** Representative traces of sIPSCs and sEPSCs from the same
895 pyramidal neuron show charge transfer measured as the area of events above
896 threshold in the aCSF control. Scale bars: 10 pA, 200 milliseconds. **(N)** Integrated

897 conductances measured between 30 - 35 minutes after addition of AD1 application
898 were normalized to the value of 5 minutes before addition of AD1. Mean excitatory
899 integrated conductance increased and mean inhibitory integrated conductance
900 decreased upon treatment of AD1 (E: excitatory input/sEPSCs; I: inhibitory
901 input/sIPSCs). Each slice used for each treatment was from a different animal. # $p <$
902 0.05, ## $p <$ 0.01.

903

904 **Figure 5. Expression of APP is required for the plasticity-disrupting activity of**
905 **A β -containing AD brain extract.**

906 **(A)** Detergent extracts of mouse brain slices used for electrophysiology were analyzed
907 for APP by Western blotting with 22C11. Full-length APP was readily detected in
908 extracts from wild type littermate mice (WT) but not APP knockout mice (APP KO).
909 Slices from 2 APP KO mice (KO1 and KO2) and 2 WT mice (WT1 and WT2) are shown.

910 **(B)** Input/output curves recorded in the hippocampal CA1 area are highly similar for
911 both WT and APP KO mouse brain slices ($p=0.19$, One-Way ANOVA). Values are
912 mean \pm SEM. **(C)** LTP recorded in hippocampal CA1 was similar in brain slices from

913 WT and APP KO mice (WT Ctr, black circles vs. APP KO Ctr, gray hexagons, $p=0.79$,
914 comparison of the last 10 minutes recording using One-Way ANOVA). However, the
915 extract from AD1 brain blocked LTP in WT but not in APP KO mice brain slices.

916 Horizontal gray bar indicates the duration in which sample was present. 1 and 2
917 indicate example traces from time points just prior to the theta burst stimulation ($\uparrow\uparrow\uparrow$
918 TBS) (1) and 60 minutes after TBS (2), respectively. The aCSF control in WT mice is

919 shown with black circles; AD1 treatment in WT mice is shown in magenta diamonds; the
920 aCSF control in APP KO mice is shown in gray hexagons and AD1 treatment in APP
921 KO mice is shown using pink upward triangles. WT slices for each treatment came from

922 different animals; the APP KO slices came from a total of 4 APP KO mice. Scale bars:
923 0.5 mV, 15 milliseconds. **(D)** Comparison of average potentiation from last 10 minutes
924 of LTP recording ($F=4.5$, $p=0.0005$, Control vs. AD1 in WT mice; $F=4.5$, $p=0.41$, Control
925 vs. AD1 in APP KO mice; One-Way ANOVA). Symbols correspond to those in panel **C**.

926 **(E)** Representative traces of averaged field recordings were collected after 5 stimulation

927 bursts (inter-stimulation interval 20 millisecond, inter-burst interval 30 seconds) before
928 (gray, aCSF) and 30 minutes after perfusion with the AD1 sample (pink) on brain slices
929 from APP KO mouse. Scale bars: 0.5 mV, 10 millisecond. (F) fEPSPs amplitude after
930 2 to 5 stimulations were normalized to the value obtained after the first stimulation.
931 There is no significant difference between aCSF control and the presence of AD1 brain
932 extract application ($n = 5$, $F=5.32$, $p=0.7$, One-Way ANOVA). Values are mean \pm SEM.
933 Each slice used for each treatment was from a different animal. ### $p<0.001$.

934

935 **Figure 6. Characterization of the aqueous extract from AD2 brain, synthetic A β**
936 **oligomers, and second APP KO mouse line. (A)** Aqueous extract of AD2 was
937 treated with either pre-immune serum or with AW7 antiserum. Portions of the mock
938 immunodepleted sample (AD2, magenta) and the AW7 immunodepleted sample (ID-
939 AD2, green) were then analyzed by IP/WB, using AW7 for IP and a combination of 2G3
940 and 21F12 (left panel), or 6E10 (right panel) for WB. As expected, recombinant A η - α
941 was detected by 6E10, but not 2G3/21F12. **M** denotes A β monomer and * indicates a
942 broad smear ~7–8 kDa. Only non-specific (NS) bands were detected above 16 kDa
943 marker. **(B)** AD2 (magenta) and ID-AD2 (green) samples were incubated +/- 5 M
944 GuHCl and analyzed using an immunoassay that preferentially recognizes A β 42
945 monomer (266-21F12b). AW7 ID reduced monomer from 6.65 ± 0.01 ng/ml to
946 undetectable level without GuHCl treatment. Upon treatment with GuHCl, the amount of
947 A β 42 increased to 46.94 ± 0.2 ng/ml in AD2 and this was reduced to 8.62 ± 0.1 ng/ml by
948 immunodepletion. **(C)** Size-exclusion chromatography of ADDLs revealed a prominent
949 high molecular weight peak, a trail of intermediate molecular weight species and a small
950 A β monomer peak. **(D)** Negative contrast electron micrograph shows mostly protofibril-
951 like structures. Scale bar is 50 nm. **(E)** Brain slices from wild type (WT) and a second
952 line of APP knock-outs (KO) were analyzed for APP by Western blotting with 22C11.
953 Full-length APP was readily detected in extracts from WT but not APP KO. Slices from
954 2 KO (KO1 and KO2) and 2 WT (WT1 and WT2) mice are shown. **(F)** Input/output
955 curves recorded in the hippocampal CA1 area are highly similar for WT and APP KO
956 mouse brain slices ($F=4.6$, $p=0.91$, One-Way ANOVA). Values are mean \pm SEM. Each
957 slice used for each treatment was from a different animal.

958 **Figure 7. A second APP KO mouse line confirms that APP is required for the**
959 **synaptic-disrupting activity of both AD brain and synthetic A β oligomers.**

960 **(A)** LTP recorded in hippocampal CA1 was similar in brain slices from WT and Zheng
961 APP KO mice. Notably, the extract from AD2 blocked LTP in brain slices from WT but
962 not APP KO mice. Horizontal gray bar indicates the duration during when sample was
963 present. 1 and 2 indicate example traces from time points just prior to the theta burst
964 stimulation ($\uparrow\uparrow\uparrow$ TBS) (1) and 60 minutes after TBS (2), respectively. The aCSF control
965 in WT mice is shown with black circles; AD2 treatment in WT mice is shown in magenta
966 diamonds; ID-AD2 treatment in WT slices in green downward triangles. The aCSF
967 control in APP KO mice is shown in gray hexagons and AD2 treatment in APP KO mice
968 is shown using pink upward triangles. WT slices for each treatment came from different
969 animals; the APP KO slices came from a total of 6 APP KO mice. Scale bars: 0.5 mV,
970 15 millisecond. **(B)** Comparison of average potentiation from last 10 minutes of LTP
971 recording ($F=4.96$, $p=0.0001$, Control vs. AD2 in WT mice; $F=5.12$, $p=0.56$, Control vs.
972 AD2 in APP KO mice; One-Way ANOVA). Symbols correspond to those in panel **A**. **(C)**
973 ADDLs blocked LTP in WT, but not in APP KO, brain slices. Horizontal gray bar
974 indicates the duration during when sample was present. 1 and 2 indicate example
975 traces from time points just prior to the theta burst stimulation ($\uparrow\uparrow\uparrow$ TBS) (1) and 60
976 minutes after TBS (2), respectively. The aCSF WT slices control is shown with black
977 circles; WT slices treated with ADDLs is in magenta diamonds; and vehicle in green
978 downward triangles. The aCSF control in APP KO mice is shown in gray hexagons and
979 ADDLs treatment in APP KO mice is shown using pink upward triangles. WT slices for

980 each treatment came from different animals; the APP KO slices came from a total of 6
981 APP KO mice. Scale bars: 0.7 mV, 15 millisecond. **(D)** Comparison of average
982 potentiation from last 10 minutes of LTP recording ($F=4.75$, $p=0.0006$, Control vs.
983 ADDLs in WT mice; $F=4.75$, $p=0.93$, Control vs. vehicle in WT mice; $F=4.84$, $p=0.07$,
984 Control vs. ADDLs in APP KO mice; One-Way ANOVA). Symbols correspond to those
985 in panel **C**. Each slice used for each treatment was from a different animal. ### $p<$
986 0.001.

987

988 **Figure 8. APP knock out occludes the effects of A β -containing AD brain extract**
989 **on both excitatory and inhibitory post-synaptic currents and rescues the**
990 **disruption of E/I balance.**

991 **(A, D)** Example traces of sEPSCs **(A)** and sIPSCs **(D)** before (aCSF, black) and 30
992 minutes after addition of AD1 extract (magenta) on WT hippocampal brain slices. Scale
993 bars: 20 pA, 700 millisecond. **(B)** Treatment with AD1 extract decreased inter-event
994 intervals and increased mean frequency (insert) of sEPSCs ($p=6.34E-15$, K-S test;
995 $p=0.003$, student's t -test; $n = 5$), but **(C)** did not significantly change the cumulative
996 distributions or the mean value (insert) of the amplitude of sEPSCs ($n = 5$) on WT slices.
997 **(E)** 30 minutes of AD1 treatment increased inter-event intervals and decreased mean
998 frequency (insert) of sIPSCs ($p=9.44E-20$, K-S test; $p=0.006$, student's t -test; $n = 5$), but
999 **(F)** did not affect the cumulative distributions or the mean value (insert) of the amplitude
1000 of sIPSCs ($n = 5$) on WT slices. **(G, J)** Example traces of spontaneous post-synaptic
1001 currents (sEPSCs, **G**; sIPSCs, **J**) before (aCSF, gray) and 30-40 minutes following
1002 addition of AD1 extract (pink) on APP KO mice hippocampal brain slices. Scale bars:
1003 20 pA, 700 millisecond. **(H)** Treatment with AD1 sample affected neither frequency nor
1004 amplitude (I) of sEPSCs ($p=0.14$, K-S test; $p=0.26$, student's t -test; $n = 6$) on APP KO
1005 mice. Similarly, treatment of APP KO neurons with AD1 did not change frequency **(K)**
1006 or the amplitude **(L, $p=0.58$, K-S test; $p=0.25$ student's t -test; $n = 6$)** of sIPSCs. **(M)**
1007 Application of A β -containing AD brain extract significantly changed the integrated
1008 conductance of both excitatory (E) and inhibitory (I) input to neurons and disrupted the
1009 E/I balance in WT animals, but not in APP KO mice ($p=0.001$, E/I in WT vs. E/I in APP
1010 KO, One-Way ANOVA).

1011 **Figure 9: A β binding to synaptic terminals requires expression of APP.**

1012 **(A)** Array tomography of hippocampi stained for synapsin-1 (pre-synapses), A β (1C22),
1013 and PSD95 (post-synapses) reveal co-localization of A β at synapses in slices incubated
1014 with AD1 brain extract. Images have been processed for analysis as described in the
1015 methods and Figure 1. **(B and C)** The amount of synaptic 1C22 staining was
1016 significantly greater in slices incubated with AD1 extract than in slices incubated with
1017 aCSF or ID-AD1 extract based on **(B)** co-localization of 1C22 and synapsin 1 staining
1018 (Kruskal Wallis test ($\chi^2_{(4)}=10.844$, $p=0.028$) Dunns *post-hoc* vs. control $p=0.021$), and **(C)**
1019 1C22 and PSD95 co-localization (Kruskal Wallis test for PSD95 ($\chi^2_{(4)}=11.583$, $p=0.021$;
1020 Dunns *post-hoc* vs. control, $p=0.01$). Importantly, when slices from APP KO mice were
1021 incubated with AD1 extract there was no significant co-localization of 1C22 staining with
1022 either synapsin 1 **(B)** (Dunns *post-hoc* vs. control, $p=1.000$) or PSD-95 **(C)** (Dunns *post-*
1023 *hoc* vs. control, $p=1.000$). Graphs represent the medians \pm the interquartile range per
1024 treatment. Each data point is derived from the analysis of $\sim 3,500$ synapses imaged per
1025 brain slice. Within each treatment group the 3 slices used were from 3 different mice **(B**
1026 **and C)**. Arrows indicate specific examples of 1C22 staining co-localizing with pre- or
1027 post-synapses. Scale bar is 2 μm in **(A)**. # $p < 0.05$.

1028 **Figure 10. APP expressing, but not APP lacking, brain slices bind synaptotoxic**
1029 **A β .**

1030 **(A)** AD2 brain extract was pre-incubated with either 4 WT or 4 APP KO brain slices for
1031 2 hours and the resultant solutions were used to perfuse WT brain slices. **(B)** Time
1032 course plots of LTP recorded in WT brain hippocampal CA1 show that AD2 brain extract
1033 pre-incubated with APP KO brains slices blocked LTP, whereas AD2 pre-incubated with
1034 WT brain slices allow normal LTP. Horizontal gray bar indicates the duration during
1035 when sample was present. 1 and 2 indicate example traces from time points just prior to
1036 the theta burst stimulation ($\uparrow\uparrow\uparrow$ TBS) (1) and 60 minutes after TBS (2), respectively.
1037 The aCSF control in WT mice is shown with black circles; AD2 incubated with APP KO
1038 brain slices in WT mice is shown in magenta diamonds; AD2 pre-incubated with WT
1039 brain slices is in green downward triangles. Scale bars: 0.5 mV, 15 millisecond. **(C)**
1040 Comparison of average potentiation from last 10 minutes of LTP recording ($F=4.96$,
1041 $p=0.003$, Control vs. APP KO slices with AD2; $F=4.96$, $p=0.82$, Control vs. WT slices
1042 with AD2; One-Way ANOVA). Symbols correspond to those in panel **B**. Each slice
1043 used for recording for each treatment was from a different animal. **##** $p<0.005$.

1044 **Figure 11. The level of APP expression influences the plasticity-disrupting**
1045 **activity of A β -containing AD brain extract.**

1046 **(A)** Detergent extracts of from WT, APP +/- and APP -/- mouse brain slices used for
1047 electrophysiology were analyzed for APP by Western blotting with 22C11. Full-length
1048 APP was readily detected in extracts from wild type mice (WT) and APP +/- mice, but
1049 not APP -/- mice. Ten μ g total protein from APP +/- slices contained a similar amount of
1050 APP as 5 μ g total protein from WT slices. **(B)** Input/output curves recorded in the
1051 hippocampal CA1 area are highly similar for both WT and APP +/- mouse brain slices
1052 ($F=4.6$, $p=0.75$, One-Way ANOVA). **(C)** LTP recorded in hippocampal CA1 was similar
1053 in brain slices from WT and APP +/- mice. However, AD2 caused a stronger block of
1054 LTP in WT slices compared with APP +/- slices. Horizontal gray bar indicates the
1055 duration during when sample was present. 1 and 2 indicate example traces from time
1056 points just prior to the theta burst stimulation ($\uparrow\uparrow\uparrow$ TBS) (1) and 60 minutes after TBS
1057 (2), respectively. The aCSF control in WT mice is shown with black circles; AD2
1058 treatment in WT mice is shown in magenta diamonds; the aCSF control in APP +/- mice
1059 is shown in gray hexagons and AD2 treatment in APP +/- mice is shown using pink
1060 upward triangles. Scale bars: 0.5 mV, 15 milliseconds. Each slice used for each
1061 treatment was from a different animal. **(D)** Comparison of average potentiation from the
1062 last 10 minutes of LTP recording ($F=4.45$, $p=0.84$, Control in WT mice vs. Control in
1063 APP +/- mice; $F=4.5$, $p=2.67E-007$, Control vs. AD2 in WT mice; $F=4.49$, $p=0.003$,
1064 Control vs. AD2 in WT mice; One-Way ANOVA). Symbols correspond to those in panel

1065 **C.** Values are mean \pm SEM. Each slice used for each treatment was from a different
1066 animal. ## $p < 0.005$, ### $p < 0.0001$.

1067

1068 **References**

1069

1070 Abramov E, Dolev I, Fogel H, Ciccotosto GD, Ruff E, Slutsky I (2009) Amyloid-beta as a positive
1071 endogenous regulator of release probability at hippocampal synapses. *Nat Neurosci* 12:1567-
1072 1576.

1073 Bai Y, Markham K, Chen F, Weerasekera R, Watts J, Horne P, Wakutani Y, Bagshaw R, Mathews PM,
1074 Fraser PE, Westaway D, St George-Hyslop P, Schmitt-Ulms G (2008) The in vivo brain
1075 interactome of the amyloid precursor protein. *Mol Cell Proteomics* 7:15-34.

1076 Barry AE, Klyubin I, Mc Donald JM, Mably AJ, Farrell MA, Scott M, Walsh DM, Rowan MJ (2011)
1077 Alzheimer's disease brain-derived amyloid-beta-mediated inhibition of LTP in vivo is prevented
1078 by immunotargeting cellular prion protein. *J Neurosci* 31:7259-7263.

1079 Betts V, Leissring MA, Dolios G, Wang R, Selkoe DJ, Walsh DM (2008) Aggregation and catabolism of
1080 disease-associated intra-Abeta mutations: reduced proteolysis of AbetaA21G by neprilysin.
1081 *Neurobiol Dis* 31:442-450.

1082 Borlikova GG, Trejo M, Mably AJ, Mc Donald JM, Sala Frigerio C, Regan CM, Murphy KJ, Masliah E, Walsh
1083 DM (2013) Alzheimer brain-derived amyloid beta-protein impairs synaptic remodeling and
1084 memory consolidation. *Neurobiol Aging* 34:1315-1327.

1085 Born HA, Kim JY, Savjani RR, Das P, Dabaghian YA, Guo Q, Yoo JW, Schuler DR, Cirrito JR, Zheng H, Golde
1086 TE, Noebels JL, Jankowsky JL (2014) Genetic suppression of transgenic APP rescues
1087 Hypersynchronous network activity in a mouse model of Alzheimer's disease. *J Neurosci* 34:3826-
1088 3840.

1089 Busche MA, Konnerth A (2015) Neuronal hyperactivity--A key defect in Alzheimer's disease? *Bioessays*
1090 37:624-632.

1091 Callahan DG, Taylor WM, Tilearcio M, Cavanaugh T, Selkoe DJ, Young-Pearse TL (2017) Embryonic
1092 mosaic deletion of APP results in displaced Reelin-expressing cells in the cerebral cortex. *Dev*
1093 *Biol* 424:138-146.

1094 Cirrito JR, Yamada KA, Finn MB, Sloviter RS, Bales KR, May PC, Schoepp DD, Paul SM, Mennerick S,
1095 Holtzman DM (2005) Synaptic activity regulates interstitial fluid amyloid-beta levels in vivo.
1096 *Neuron* 48:913-922.

1097 Cleary JP, Walsh DM, Hofmeister JJ, Shankar GM, Kuskowski MA, Selkoe DJ, Ashe KH (2005) Natural
1098 oligomers of the amyloid-beta protein specifically disrupt cognitive function. *Nat Neurosci* 8:79-
1099 84.

1100 Conboy L, Murphy KJ, Regan CM (2005) Amyloid precursor protein expression in the rat hippocampal
1101 dentate gyrus modulates during memory consolidation. *J Neurochem* 95:1677-1688.

1102 Dawson GR, Seabrook GR, Zheng H, Smith DW, Graham S, O'Dowd G, Bowery BJ, Boyce S, Trumbauer
1103 ME, Chen HY, Van der Ploeg LH, Sirinathsinghji DJ (1999) Age-related cognitive deficits, impaired
1104 long-term potentiation and reduction in synaptic marker density in mice lacking the beta-
1105 amyloid precursor protein. *Neuroscience* 90:1-13.

1106 De Strooper B (2010) Proteases and proteolysis in Alzheimer disease: a multifactorial view on the
1107 disease process. *Physiol Rev* 90:465-494.

1108 DeFelipe J (2002) Cortical interneurons: from Cajal to 2001. *Prog Brain Res* 136:215-238.

1109 Del Prete D, Lombino F, Liu X, D'Adamio L (2014) APP is cleaved by Bace1 in pre-synaptic vesicles and
1110 establishes a pre-synaptic interactome, via its intracellular domain, with molecular complexes
1111 that regulate pre-synaptic vesicles functions. *PLoS One* 9:e108576.

1112 Del Turco D, Paul MH, Schlaudraff J, Hick M, Endres K, Muller UC, Deller T (2016) Region-Specific
1113 Differences in Amyloid Precursor Protein Expression in the Mouse Hippocampus. *Front Mol*
1114 *Neurosci* 9:134.

1115 Doyle E, Bruce MT, Breen KC, Smith DC, Anderton B, Regan CM (1990) Intraventricular infusions of
1116 antibodies to amyloid-beta-protein precursor impair the acquisition of a passive avoidance
1117 response in the rat. *Neurosci Lett* 115:97-102.

1118 Fanutza T, Del Prete D, Ford MJ, Castillo PE, D'Adamio L (2015) APP and APLP2 interact with the synaptic
1119 release machinery and facilitate transmitter release at hippocampal synapses. *Elife* 4:e09743.

1120 Fogel H, Frere S, Segev O, Bharill S, Shapira I, Gazit N, O'Malley T, Slomowitz E, Berdichevsky Y, Walsh
1121 DM, Isacoff EY, Hirsch JA, Slutsky I (2014) APP homodimers transduce an amyloid-beta-mediated
1122 increase in release probability at excitatory synapses. *Cell Rep* 7:1560-1576.

1123 Fowler SW, Chiang AC, Savjani RR, Larson ME, Sherman MA, Schuler DR, Cirrito JR, Lesne SE, Jankowsky
1124 JL (2014) Genetic modulation of soluble Abeta rescues cognitive and synaptic impairment in a
1125 mouse model of Alzheimer's disease. *J Neurosci* 34:7871-7885.

1126 Freir DB, Nicoll AJ, Klyubin I, Panico S, Mc Donald JM, Risse E, Asante EA, Farrow MA, Sessions RB, Saibil
1127 HR, Clarke AR, Rowan MJ, Walsh DM, Collinge J (2011) Interaction between prion protein and
1128 toxic amyloid beta assemblies can be therapeutically targeted at multiple sites. *Nat Commun*
1129 2:336.

1130 Garcia-Marin V, Blazquez-Llorca L, Rodriguez JR, Boluda S, Muntane G, Ferrer I, Defelipe J (2009)
1131 Diminished perisomatic GABAergic terminals on cortical neurons adjacent to amyloid plaques.
1132 *Front Neuroanat* 3:28.

1133 Gillespie AK, Jones EA, Lin YH, Karlsson MP, Kay K, Yoon SY, Tong LM, Nova P, Carr JS, Frank LM, Huang Y
1134 (2016) Apolipoprotein E4 Causes Age-Dependent Disruption of Slow Gamma Oscillations during
1135 Hippocampal Sharp-Wave Ripples. *Neuron* 90:740-751.

1136 Guerreiro R, Hardy J (2014) Genetics of Alzheimer's disease. *Neurotherapeutics* 11:732-737.

1137 Hartley DM, Walsh DM, Ye CP, Diehl T, Vasquez S, Vassilev PM, Teplow DB, Selkoe DJ (1999)
1138 Protofibrillar intermediates of amyloid beta-protein induce acute electrophysiological changes
1139 and progressive neurotoxicity in cortical neurons. *J Neurosci* 19:8876-8884.

1140 Hsieh H, Boehm J, Sato C, Iwatsubo T, Tomita T, Sisodia S, Malinow R (2006) AMPAR removal underlies
1141 Abeta-induced synaptic depression and dendritic spine loss. *Neuron* 52:831-843.

1142 Huang JK, Ma PL, Ji SY, Zhao XL, Tan JX, Sun XJ, Huang FD (2013) Age-dependent alterations in the
1143 presynaptic active zone in a Drosophila model of Alzheimer's disease. *Neurobiol Dis* 51:161-167.

1144 Huber G, Martin JR, Loffler J, Moreau JL (1993) Involvement of amyloid precursor protein in memory
1145 formation in the rat: an indirect antibody approach. *Brain Res* 603:348-352.

1146 Jedlicka P, Owen M, Vnencak M, Tschape JA, Hick M, Muller UC, Deller T (2012) Functional
1147 consequences of the lack of amyloid precursor protein in the mouse dentate gyrus in vivo. *Exp*
1148 *Brain Res* 217:441-447.

1149 Jo S et al. (2014) GABA from reactive astrocytes impairs memory in mouse models of Alzheimer's
1150 disease. *Nat Med* 20:886-896.

1151 Johnson KA, Fox NC, Sperling RA, Klunk WE (2012) Brain imaging in Alzheimer disease. *Cold Spring Harb*
1152 *Perspect Med* 2:a006213.

1153 Kabogo D, Rauw G, Amritraj A, Baker G, Kar S (2010) ss-amyloid-related peptides potentiate K⁺-evoked
1154 glutamate release from adult rat hippocampal slices. *Neurobiol Aging* 31:1164-1172.

1155 Kamenetz F, Tomita T, Hsieh H, Seabrook G, Borchelt D, Iwatsubo T, Sisodia S, Malinow R (2003) APP
1156 processing and synaptic function. *Neuron* 37:925-937.

1157 Kay KR, Smith C, Wright AK, Serrano-Pozo A, Pooler AM, Koffie R, Bastin ME, Bak TH, Abrahams S,
1158 Kopeikina KJ, McGuone D, Frosch MP, Gillingwater TH, Hyman BT, Spires-Jones TL (2013)
1159 Studying synapses in human brain with array tomography and electron microscopy. *Nat Protoc*
1160 8:1366-1380.

1161 Kirouac L, Rajic AJ, Cribbs DH, Padmanabhan J (2017) Activation of Ras-ERK Signaling and GSK-3 by
1162 Amyloid Precursor Protein and Amyloid Beta Facilitates Neurodegeneration in Alzheimer's
1163 Disease. *eNeuro* 4.

1164 Klyubin I, Cullen WK, Hu NW, Rowan MJ (2012) Alzheimer's disease Abeta assemblies mediating rapid
1165 disruption of synaptic plasticity and memory. *Mol Brain* 5:25.

1166 Klyubin I, Betts V, Welzel AT, Blennow K, Zetterberg H, Wallin A, Lemere CA, Cullen WK, Peng Y,
1167 Wisniewski T, Selkoe DJ, Anwyl R, Walsh DM, Rowan MJ (2008) Amyloid beta protein dimer-
1168 containing human CSF disrupts synaptic plasticity: prevention by systemic passive immunization.
1169 *J Neurosci* 28:4231-4237.

1170 Koffie RM, Meyer-Luehmann M, Hashimoto T, Adams KW, Mielke ML, Garcia-Alloza M, Micheva KD,
1171 Smith SJ, Kim ML, Lee VM, Hyman BT, Spires-Jones TL (2009) Oligomeric amyloid beta associates
1172 with postsynaptic densities and correlates with excitatory synapse loss near senile plaques. *Proc*
1173 *Natl Acad Sci U S A* 106:4012-4017.

1174 Koffie RM, Hashimoto T, Tai HC, Kay KR, Serrano-Pozo A, Joyner D, Hou S, Kopeikina KJ, Frosch MP, Lee
1175 VM, Holtzman DM, Hyman BT, Spires-Jones TL (2012) Apolipoprotein E4 effects in Alzheimer's
1176 disease are mediated by synaptotoxic oligomeric amyloid-beta. *Brain* 135:2155-2168.

1177 Kohli BM, Pflieger D, Mueller LN, Carbonetti G, Aebbersold R, Nitsch RM, Konietzko U (2012) Interactome
1178 of the amyloid precursor protein APP in brain reveals a protein network involved in synaptic
1179 vesicle turnover and a close association with Synaptotagmin-1. *J Proteome Res* 11:4075-4090.

1180 Kurudenkandy FR, Zilberter M, Biverstal H, Presto J, Honcharenko D, Stromberg R, Johansson J, Winblad
1181 B, Fisahn A (2014) Amyloid-beta-induced action potential desynchronization and degradation of
1182 hippocampal gamma oscillations is prevented by interference with peptide conformation
1183 change and aggregation. *J Neurosci* 34:11416-11425.

1184 Lacor PN, Buniel MC, Furlow PW, Clemente AS, Velasco PT, Wood M, Viola KL, Klein WL (2007) Abeta
1185 oligomer-induced aberrations in synapse composition, shape, and density provide a molecular
1186 basis for loss of connectivity in Alzheimer's disease. *J Neurosci* 27:796-807.

1187 Lacor PN, Buniel MC, Chang L, Fernandez SJ, Gong Y, Viola KL, Lambert MP, Velasco PT, Bigio EH, Finch
1188 CE, Krafft GA, Klein WL (2004) Synaptic targeting by Alzheimer's-related amyloid beta oligomers.
1189 *J Neurosci* 24:10191-10200.

1190 Lambert MP, Barlow AK, Chromy BA, Edwards C, Freed R, Liosatos M, Morgan TE, Rozovsky I, Trommer B,
1191 Viola KL, Wals P, Zhang C, Finch CE, Krafft GA, Klein WL (1998) Diffusible, nonfibrillar ligands
1192 derived from Abeta1-42 are potent central nervous system neurotoxins. *Proc Natl Acad Sci U S A*
1193 95:6448-6453.

1194 Lassek M, Weingarten J, Einsfelder U, Brendel P, Muller U, Volkandt W (2013) Amyloid precursor
1195 proteins are constituents of the presynaptic active zone. *J Neurochem* 127:48-56.

1196 Lassek M, Weingarten J, Acker-Palmer A, Bajjalieh SM, Muller U, Volkandt W (2014) Amyloid precursor
1197 protein knockout diminishes synaptic vesicle proteins at the presynaptic active zone in mouse
1198 brain. *Curr Alzheimer Res* 11:971-980.

1199 Lassek M, Weingarten J, Wegner M, Mueller BF, Rohmer M, Baeumlisberger D, Arrey TN, Hick M,
1200 Ackermann J, Acker-Palmer A, Koch I, Muller U, Karas M, Volkandt W (2016) APP Is a Context-
1201 Sensitive Regulator of the Hippocampal Presynaptic Active Zone. *PLoS Comput Biol* 12:e1004832.

1202 Lauren J, Gimbel DA, Nygaard HB, Gilbert JW, Strittmatter SM (2009) Cellular prion protein mediates
1203 impairment of synaptic plasticity by amyloid-beta oligomers. *Nature* 457:1128-1132.

1204 Lesne S, Koh MT, Kotilinek L, Kaye R, Glabe CG, Yang A, Gallagher M, Ashe KH (2006) A specific amyloid-
1205 beta protein assembly in the brain impairs memory. *Nature* 440:352-357.

1206 Li S, Hong S, Shepardson NE, Walsh DM, Shankar GM, Selkoe D (2009) Soluble oligomers of amyloid Beta
1207 protein facilitate hippocampal long-term depression by disrupting neuronal glutamate uptake.
1208 *Neuron* 62:788-801.

1209 Li S, Jin M, Koeglsperger T, Shepardson NE, Shankar GM, Selkoe DJ (2011) Soluble Abeta oligomers
1210 inhibit long-term potentiation through a mechanism involving excessive activation of
1211 extrasynaptic NR2B-containing NMDA receptors. *J Neurosci* 31:6627-6638.

1212 Lillis KP, Wang Z, Mail M, Zhao GQ, Berdichevsky Y, Bacskai B, Staley KJ (2015) Evolution of Network
1213 Synchronization during Early Epileptogenesis Parallels Synaptic Circuit Alterations. *J Neurosci*
1214 35:9920-9934.

1215 Lorenzo A, Yuan M, Zhang Z, Paganetti PA, Sturchler-Pierrat C, Staufenbiel M, Mautino J, Vigo FS,
1216 Sommer B, Yankner BA (2000) Amyloid beta interacts with the amyloid precursor protein: a
1217 potential toxic mechanism in Alzheimer's disease. *Nat Neurosci* 3:460-464.

1218 Mably AJ, Kanmert D, Mc Donald JM, Liu W, Caldarone BJ, Lemere CA, O'Nuallain B, Kosik KS, Walsh DM
1219 (2015) Tau immunization: a cautionary tale? *Neurobiol Aging* 36:1316-1332.

1220 Mc Donald JM, O'Malley TT, Liu W, Mably AJ, Brinkmalm G, Portelius E, Wittbold WM, 3rd, Frosch MP,
1221 Walsh DM (2015) The aqueous phase of Alzheimer's disease brain contains assemblies built
1222 from approximately 4 and approximately 7 kDa Abeta species. *Alzheimers Dement* 11:1286-
1223 1305.

1224 Melchor JP, Van Nostrand WE (2000) Fibrillar amyloid beta-protein mediates the pathologic
1225 accumulation of its secreted precursor in human cerebrovascular smooth muscle cells. *J Biol*
1226 *Chem* 275:9782-9791.

1227 Melnikova T, Fromholt S, Kim H, Lee D, Xu G, Price A, Moore BD, Golde TE, Felsenstein KM, Savonenko A,
1228 Borchelt DR (2013) Reversible pathologic and cognitive phenotypes in an inducible model of
1229 Alzheimer-amyloidosis. *J Neurosci* 33:3765-3779.

1230 Mileusnic R, Lancashire CL, Johnston AN, Rose SP (2000) APP is required during an early phase of
1231 memory formation. *Eur J Neurosci* 12:4487-4495.

1232 Minkeviciene R, Rheims S, Dobszay MB, Zilberter M, Hartikainen J, Fulop L, Penke B, Zilberter Y, Harkany
1233 T, Pitkanen A, Tanila H (2009) Amyloid beta-induced neuronal hyperexcitability triggers
1234 progressive epilepsy. *J Neurosci* 29:3453-3462.

1235 Mockett BG, Richter M, Abraham WC, Muller UC (2017) Therapeutic Potential of Secreted Amyloid
1236 Precursor Protein APPsalpha. *Front Mol Neurosci* 10:30.

1237 Muller UC, Zheng H (2012) Physiological functions of APP family proteins. *Cold Spring Harb Perspect*
1238 *Med* 2:a006288.

1239 Neve RL, McPhie DL (2007) Dysfunction of amyloid precursor protein signaling in neurons leads to DNA
1240 synthesis and apoptosis. *Biochim Biophys Acta* 1772:430-437.

1241 Nimmrich V, Grimm C, Draguhn A, Barghorn S, Lehmann A, Schoemaker H, Hillen H, Gross G, Ebert U,
1242 Bruehl C (2008) Amyloid beta oligomers (A beta(1-42) globulomer) suppress spontaneous
1243 synaptic activity by inhibition of P/Q-type calcium currents. *J Neurosci* 28:788-797.

1244 Ollion J, Cochennec J, Loll F, Escude C, Boudier T (2013) TANGO: a generic tool for high-throughput 3D
1245 image analysis for studying nuclear organization. *Bioinformatics* 29:1840-1841.

1246 Palop JJ, Mucke L (2010) Amyloid-beta-induced neuronal dysfunction in Alzheimer's disease: from
1247 synapses toward neural networks. *Nat Neurosci* 13:812-818.

1248 Palop JJ, Mucke L (2016) Network abnormalities and interneuron dysfunction in Alzheimer disease. *Nat*
1249 *Rev Neurosci* 17:777-792.

1250 Parodi J, Sepulveda FJ, Roa J, Opazo C, Inestrosa NC, Aguayo LG (2010) Beta-amyloid causes depletion of
1251 synaptic vesicles leading to neurotransmission failure. *J Biol Chem* 285:2506-2514.

1252 Pickett EK, Koffie RM, Wegmann S, Henstridge CM, Herrmann AG, Colom-Cadena M, Lleo A, Kay KR,
1253 Vaught M, Soberman R, Walsh DM, Hyman BT, Spires-Jones TL (2016) Non-Fibrillar Oligomeric
1254 Amyloid-beta within Synapses. *J Alzheimers Dis* 53:787-800.

1255 Pliassova A, Lopes JP, Lemos C, Oliveira CR, Cunha RA, Agostinho P (2016) The Association of Amyloid-
1256 beta Protein Precursor With alpha- and beta-Secretases in Mouse Cerebral Cortex Synapses Is
1257 Altered in Early Alzheimer's Disease. *Mol Neurobiol* 53:5710-5721.

1258 Portelius E, Olsson M, Brinkmalm G, Ruetschi U, Mattsson N, Andreasson U, Gobom J, Brinkmalm A,
1259 Holttä M, Blennow K, Zetterberg H (2013) Mass spectrometric characterization of amyloid-beta
1260 species in the 7PA2 cell model of Alzheimer's disease. *J Alzheimers Dis* 33:85-93.

1261 Ring S, Weyer SW, Kilian SB, Waldron E, Pietrzik CU, Filippov MA, Herms J, Buchholz C, Eckman CB, Korte
1262 M, Wolfer DP, Müller UC (2007) The secreted beta-amyloid precursor protein ectodomain APPs
1263 alpha is sufficient to rescue the anatomical, behavioral, and electrophysiological abnormalities
1264 of APP-deficient mice. *J Neurosci* 27:7817-7826.

1265 Ripoli C, Piacentini R, Riccardi E, Leone L, Li Puma DD, Bitan G, Grassi C (2013) Effects of different
1266 amyloid beta-protein analogues on synaptic function. *Neurobiol Aging* 34:1032-1044.

1267 Russell CL, Semerdjieva S, Empson RM, Austen BM, Beesley PW, Alifragis P (2012) Amyloid-beta acts as a
1268 regulator of neurotransmitter release disrupting the interaction between synaptophysin and
1269 VAMP2. *PLoS One* 7:e43201.

1270 Scheff SW, Price DA, Schmitt FA, Mufson EJ (2006) Hippocampal synaptic loss in early Alzheimer's
1271 disease and mild cognitive impairment. *Neurobiol Aging* 27:1372-1384.

1272 Scheff SW, Price DA, Schmitt FA, DeKosky ST, Mufson EJ (2007) Synaptic alterations in CA1 in mild
1273 Alzheimer disease and mild cognitive impairment. *Neurology* 68:1501-1508.

1274 Schindelin J, Arganda-Carreras I, Frise E, Kaynig V, Longair M, Pietzsch T, Preibisch S, Rueden C, Saalfeld S,
1275 Schmid B, Tinevez JY, White DJ, Hartenstein V, Eliceiri K, Tomancak P, Cardona A (2012) Fiji: an
1276 open-source platform for biological-image analysis. *Nat Methods* 9:676-682.

1277 Schwenk J, Perez-Garci E, Schneider A, Kollwe A, Gauthier-Kemper A, Fritzius T, Raveh A, Dinamarca MC,
1278 Hanuschkin A, Bildl W, Klingauf J, Gassmann M, Schulte U, Bettler B, Fakler B (2016) Modular
1279 composition and dynamics of native GABAB receptors identified by high-resolution proteomics.
1280 *Nat Neurosci* 19:233-242.

1281 Seabrook GR, Smith DW, Bowery BJ, Easter A, Reynolds T, Fitzjohn SM, Morton RA, Zheng H, Dawson GR,
1282 Sirinathsinghji DJ, Davies CH, Collingridge GL, Hill RG (1999) Mechanisms contributing to the
1283 deficits in hippocampal synaptic plasticity in mice lacking amyloid precursor protein.
1284 *Neuropharmacology* 38:349-359.

1285 Shaked GM, Kummer MP, Lu DC, Galvan V, Bredesen DE, Koo EH (2006) Abeta induces cell death by
1286 direct interaction with its cognate extracellular domain on APP (APP 597-624). *FASEB J* 20:1254-
1287 1256.

1288 Shankar GM, Welzel AT, McDonald JM, Selkoe DJ, Walsh DM (2011) Isolation of low-n amyloid beta-
1289 protein oligomers from cultured cells, CSF, and brain. *Methods Mol Biol* 670:33-44.

1290 Shankar GM, Li S, Mehta TH, Garcia-Munoz A, Shepardson NE, Smith I, Brett FM, Farrell MA, Rowan MJ,
1291 Lemere CA, Regan CM, Walsh DM, Sabatini BL, Selkoe DJ (2008) Amyloid-beta protein dimers
1292 isolated directly from Alzheimer's brains impair synaptic plasticity and memory. *Nat Med*
1293 14:837-842.

1294 Soba P, Eggert S, Wagner K, Zentgraf H, Siehl K, Kreger S, Lower A, Langer A, Merdes G, Paro R, Masters
1295 CL, Müller U, Kins S, Beyreuther K (2005) Homo- and heterodimerization of APP family members
1296 promotes intercellular adhesion. *EMBO J* 24:3624-3634.

1297 Sokolow S, Luu SH, Nandy K, Miller CA, Vinters HV, Poon WW, Gylys KH (2012) Preferential accumulation
1298 of amyloid-beta in presynaptic glutamatergic terminals (VGLUT1 and VGLUT2) in Alzheimer's
1299 disease cortex. *Neurobiol Dis* 45:381-387.

1300 Sola Vigo F, Kedikian G, Heredia L, Heredia F, Anel AD, Rosa AL, Lorenzo A (2009) Amyloid-beta precursor
1301 protein mediates neuronal toxicity of amyloid beta through Go protein activation. *Neurobiol*
1302 *Aging* 30:1379-1392.

1303 Steinbach JP, Muller U, Leist M, Li ZW, Nicotera P, Aguzzi A (1998) Hypersensitivity to seizures in beta-
1304 amyloid precursor protein deficient mice. *Cell Death Differ* 5:858-866.

1305 Tamayev R, Matsuda S, Arancio O, D'Adamio L (2012) beta- but not gamma-secretase proteolysis of APP
1306 causes synaptic and memory deficits in a mouse model of dementia. *EMBO Mol Med* 4:171-179.

1307 Tanzi RE (2012) The genetics of Alzheimer disease. *Cold Spring Harb Perspect Med* 2.

1308 Van Nostrand WE, Melchor JP, Keane DM, Saporito-Irwin SM, Romanov G, Davis J, Xu F (2002)
1309 Localization of a fibrillar amyloid beta-protein binding domain on its precursor. *J Biol Chem*
1310 277:36392-36398.

1311 Vertkin I, Styr B, Slomowitz E, Ofir N, Shapira I, Berner D, Fedorova T, Laviv T, Barak-Broner N, Greitzer-
1312 Antes D, Gassmann M, Bettler B, Lotan I, Slutsky I (2015) GABAB receptor deficiency causes
1313 failure of neuronal homeostasis in hippocampal networks. *Proc Natl Acad Sci U S A* 112:E3291-
1314 3299.

1315 Walsh DM, Teplow DB (2012) Alzheimer's disease and the amyloid beta-protein. *Prog Mol Biol Transl Sci*
1316 107:101-124.

1317 Walsh DM, Klyubin I, Fadeeva JV, Cullen WK, Anwyl R, Wolfe MS, Rowan MJ, Selkoe DJ (2002) Naturally
1318 secreted oligomers of amyloid beta protein potently inhibit hippocampal long-term potentiation
1319 in vivo. *Nature* 416:535-539.

1320 Wang B, Wang Z, Sun L, Yang L, Li H, Cole AL, Rodriguez-Rivera J, Lu HC, Zheng H (2014) The amyloid
1321 precursor protein controls adult hippocampal neurogenesis through GABAergic interneurons. *J*
1322 *Neurosci* 34:13314-13325.

1323 Wang HW, Pasternak JF, Kuo H, Ristic H, Lambert MP, Chromy B, Viola KL, Klein WL, Stine WB, Krafft GA,
1324 Trommer BL (2002) Soluble oligomers of beta amyloid (1-42) inhibit long-term potentiation but
1325 not long-term depression in rat dentate gyrus. *Brain Res* 924:133-140.

1326 Wang ZM, Qi YJ, Wu PY, Zhu Y, Dong YL, Cheng ZX, Zhu YH, Dong Y, Ma L, Zheng P (2008) Neuroactive
1327 steroid pregnenolone sulphate inhibits long-term potentiation via activation of alpha2-
1328 adrenoreceptors at excitatory synapses in rat medial prefrontal cortex. *Int J*
1329 *Neuropsychopharmacol* 11:611-624.

1330 Welzel AT, Maggio JE, Shankar GM, Walker DE, Ostaszewski BL, Li S, Klyubin I, Rowan MJ, Seubert P,
1331 Walsh DM, Selkoe DJ (2014) Secreted amyloid beta-proteins in a cell culture model include N-
1332 terminally extended peptides that impair synaptic plasticity. *Biochemistry* 53:3908-3921.

1333 White AR, Zheng H, Galatis D, Maher F, Hesse L, Multhaup G, Beyreuther K, Masters CL, Cappai R (1998)
1334 Survival of cultured neurons from amyloid precursor protein knock-out mice against Alzheimer's
1335 amyloid-beta toxicity and oxidative stress. *J Neurosci* 18:6207-6217.

1336 Wilhelm BG, Mandad S, Truckenbrodt S, Krohnert K, Schafer C, Rammner B, Koo SJ, Classen GA, Krauss
1337 M, Haucke V, Urlaub H, Rizzoli SO (2014) Composition of isolated synaptic boutons reveals the
1338 amounts of vesicle trafficking proteins. *Science* 344:1023-1028.

1339 Willem M et al. (2015) eta-Secretase processing of APP inhibits neuronal activity in the hippocampus.
1340 *Nature* 526:443-447.

1341 Yang L, Wang Z, Wang B, Justice NJ, Zheng H (2009) Amyloid precursor protein regulates Cav1.2 L-type
1342 calcium channel levels and function to influence GABAergic short-term plasticity. *J Neurosci*
1343 29:15660-15668.

- 1344 Yang T, Li S, Xu H, Walsh DM, Selkoe DJ (2017) Large Soluble Oligomers of Amyloid beta-Protein from
1345 Alzheimer Brain Are Far Less Neuroactive Than the Smaller Oligomers to Which They Dissociate.
1346 J Neurosci 37:152-163.
- 1347 Yang T, O'Malley TT, Kanmert D, Jeretic J, Zieske LR, Zetterberg H, Hyman BT, Walsh DM, Selkoe DJ
1348 (2015) A highly sensitive novel immunoassay specifically detects low levels of soluble Abeta
1349 oligomers in human cerebrospinal fluid. Alzheimers Res Ther 7:14.
- 1350 Yankner BA, Lu T (2009) Amyloid beta-protein toxicity and the pathogenesis of Alzheimer disease. J Biol
1351 Chem 284:4755-4759.
- 1352 Zhang D, Mably AJ, Walsh DM, Rowan MJ (2016) Peripheral Interventions Enhancing Brain Glutamate
1353 Homeostasis Relieve Amyloid beta- and TNFalpha- Mediated Synaptic Plasticity Disruption in the
1354 Rat Hippocampus. Cereb Cortex.
- 1355 Zheng H, Jiang M, Trumbauer ME, Sirinathsinghji DJ, Hopkins R, Smith DW, Heavens RP, Dawson GR,
1356 Boyce S, Conner MW, Stevens KA, Slunt HH, Sisoda SS, Chen HY, Van der Ploeg LH (1995) beta-
1357 Amyloid precursor protein-deficient mice show reactive gliosis and decreased locomotor activity.
1358 Cell 81:525-531.
- 1359 Zucker RS, Regehr WG (2002) Short-term synaptic plasticity. Annu Rev Physiol 64:355-405.
- 1360
- 1361

Table 1. Primary and secondary antibodies.

| Antibody | Type | Antigen/epitope | Dilution for IP | Conc. For WB | Conc. For ELISA | Dilution for AT | Source/Reference |
|----------|------------|--------------------------------|-----------------|--------------|-----------------|-----------------|------------------------------------|
| 3D6 | Monoclonal | A β 1–5 | – | - | 1 μ g/ml | – | Elan/(Johnson-Wood et al., 1997) |
| 6E10 | Monoclonal | A β 3-8 | - | 1 μ g/ml | - | - | Biolegend/(Kim et al. 1988) |
| 266 | Monoclonal | A β 16-23 | – | - | 3 μ g/ml | – | Elan/(Seubert et al., 1992) |
| 2G3 | Monoclonal | A β terminating at Val40 | – | 1 μ g/ml | – | – | Elan/(Johnson-Wood et al., 1997) |
| 21F12 | Monoclonal | A β terminating at Ile42 | – | 1 μ g/ml | 1 μ g/ml | – | Elan/(Johnson-Wood et al., 1997) |
| 1C22 | Monoclonal | A β aggregates | – | – | 3 μ g/ml | 1:50 | Walsh lab/(Mably et al., 2015) |
| AW7 | Polyclonal | Pan anti-A β | 1:80 | – | – | – | Walsh lab/(Mc Donald et al., 2012) |
| 22C11 | Monoclonal | APP66-81 | – | 1 μ g/ml | – | 1:50 | Millipore/(Austin et al., 2009) |
| AB1543P | Polyclonal | Rabbit anti-synapsin-1 | – | – | – | 1:100 | Millipore/(Kay et al., 2013) |
| 3450P | Polyclonal | Rabbit anti-PSD95 | – | – | – | 1:50 | Cell Signaling/(Kay et al., 2013) |
| A21202 | Polyclonal | Donkey anti-mouse 488 | – | – | – | 1:50 | Invitrogen |
| A21207 | Polyclonal | Donkey anti-rabbit 594 | – | – | – | 1:50 | Invitrogen |
| T6074 | Monoclonal | Anti- α -Tubulin | – | 1 μ g/ml | – | – | Sigma |

Figure 1: Processing of array tomography images.

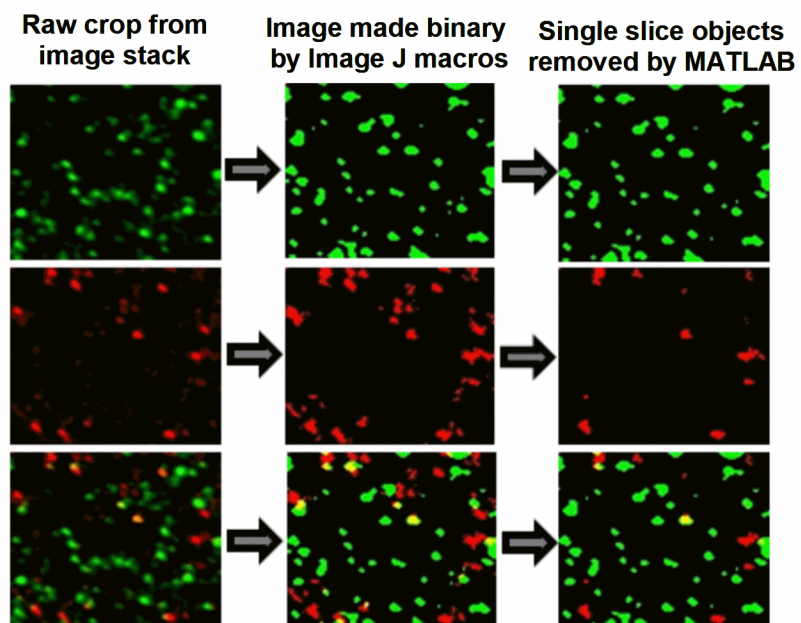


Figure 2: The water-soluble extract of AD brain, but not normal control, contains both A β monomers and oligomers and perturbs long-term synaptic plasticity.

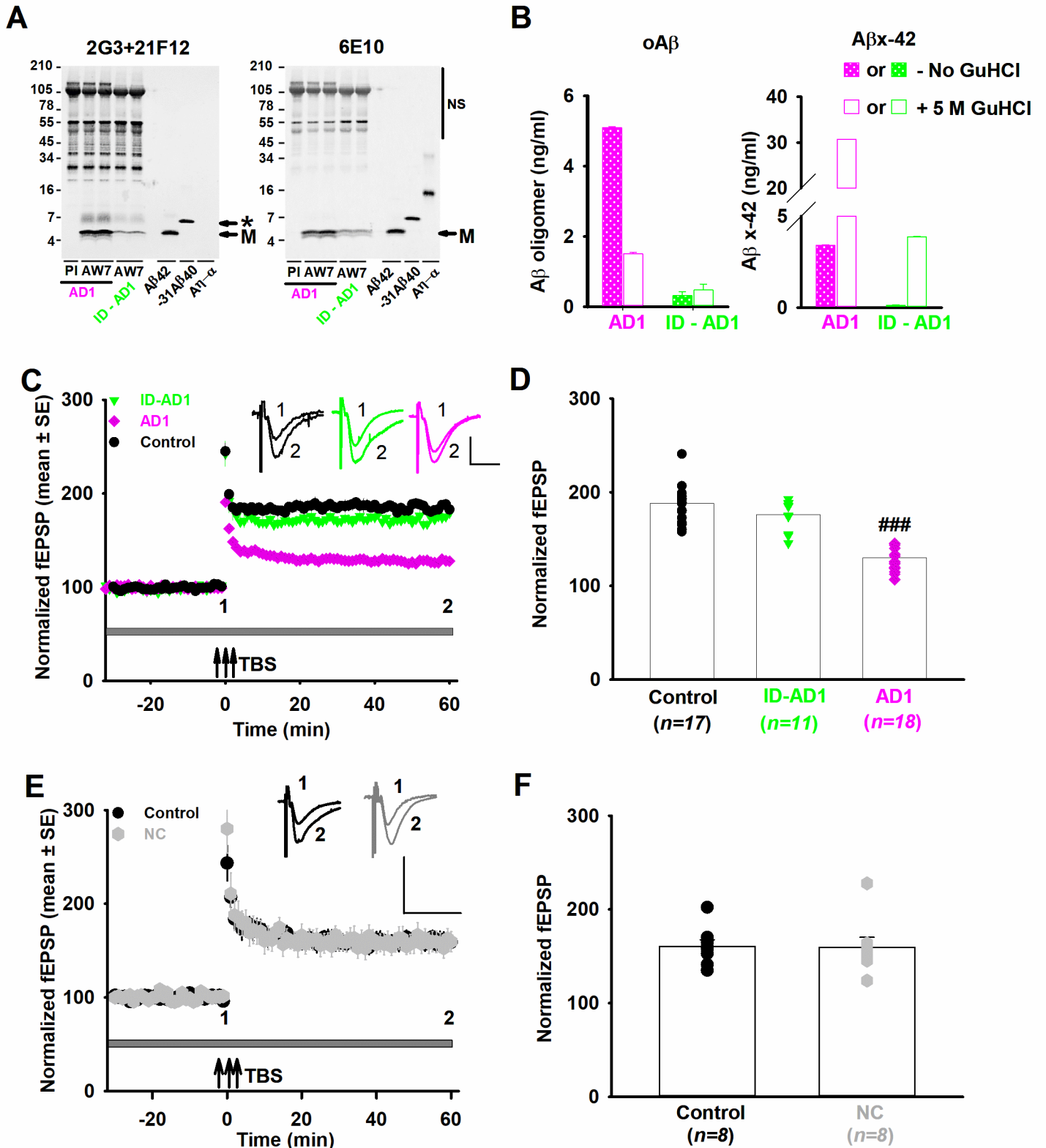


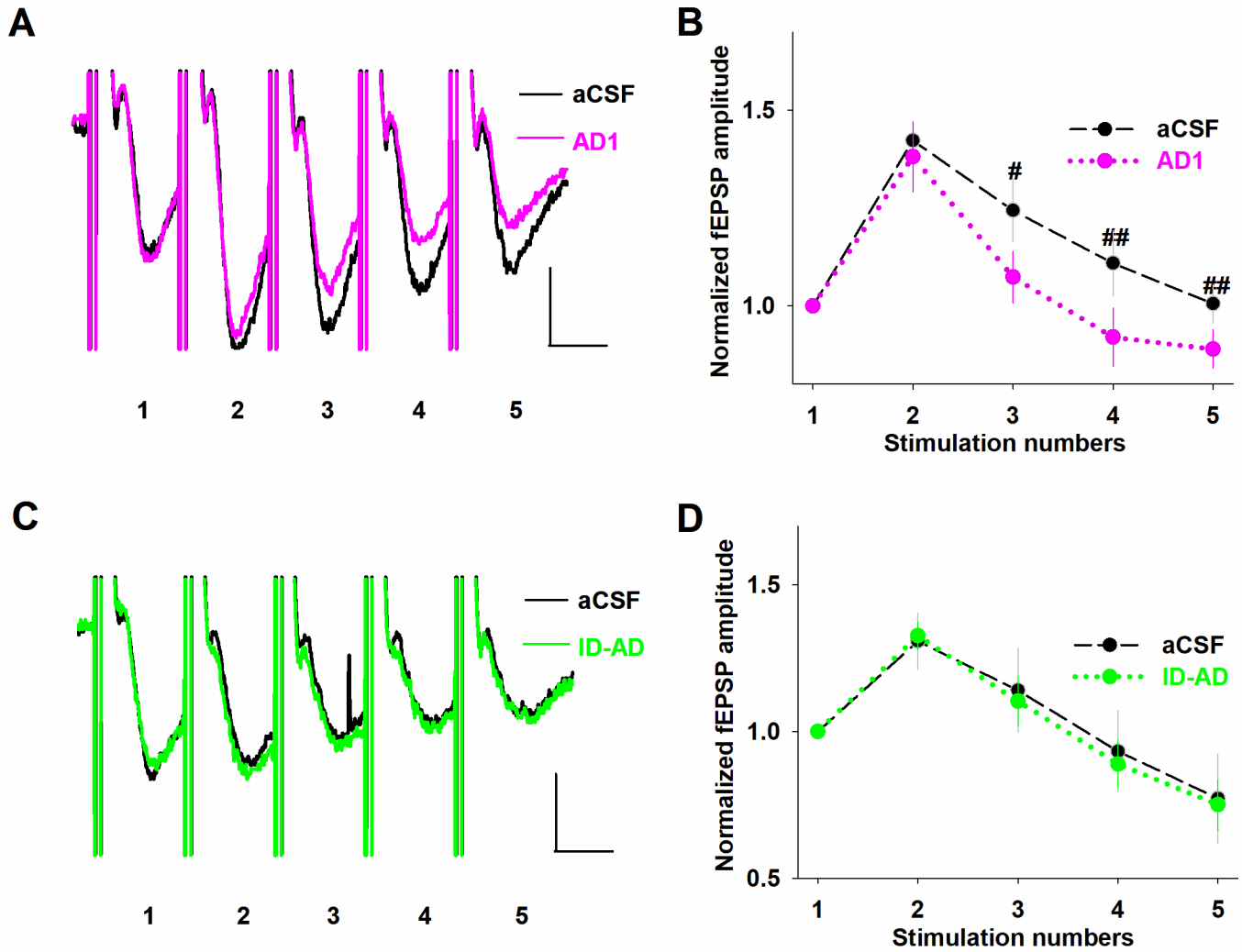
Figure 3: The A β -containing water-soluble extract of AD1 perturbs short-term facilitation.

Figure 4: AD brain-derived A β affects both excitatory and inhibitory synaptic inputs, causing disruption of the excitatory/inhibitory ratio at individual CA1 neurons.

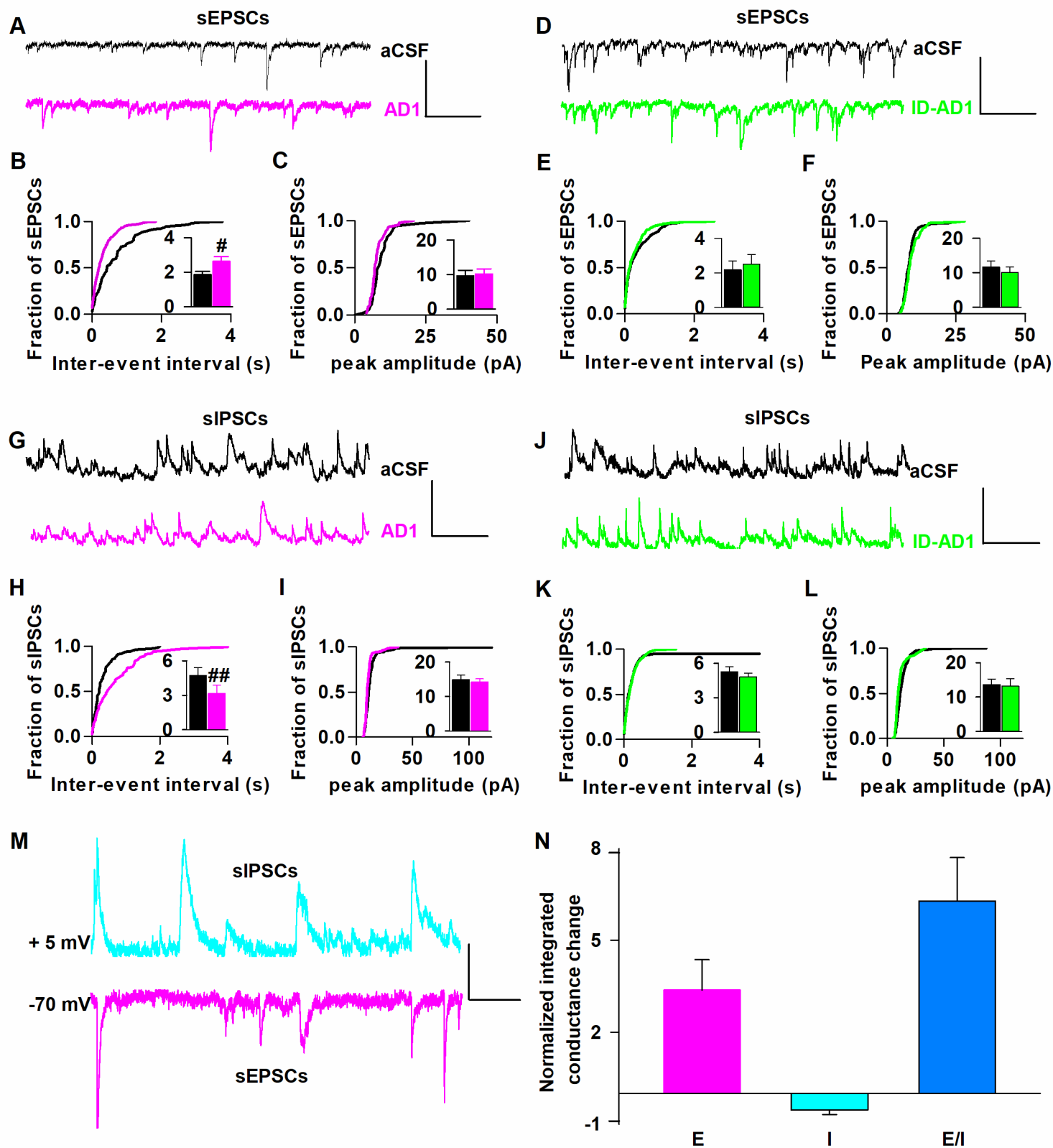


Figure 5: Expression of APP is required for the plasticity-disrupting activity of A β -containing AD brain extract.

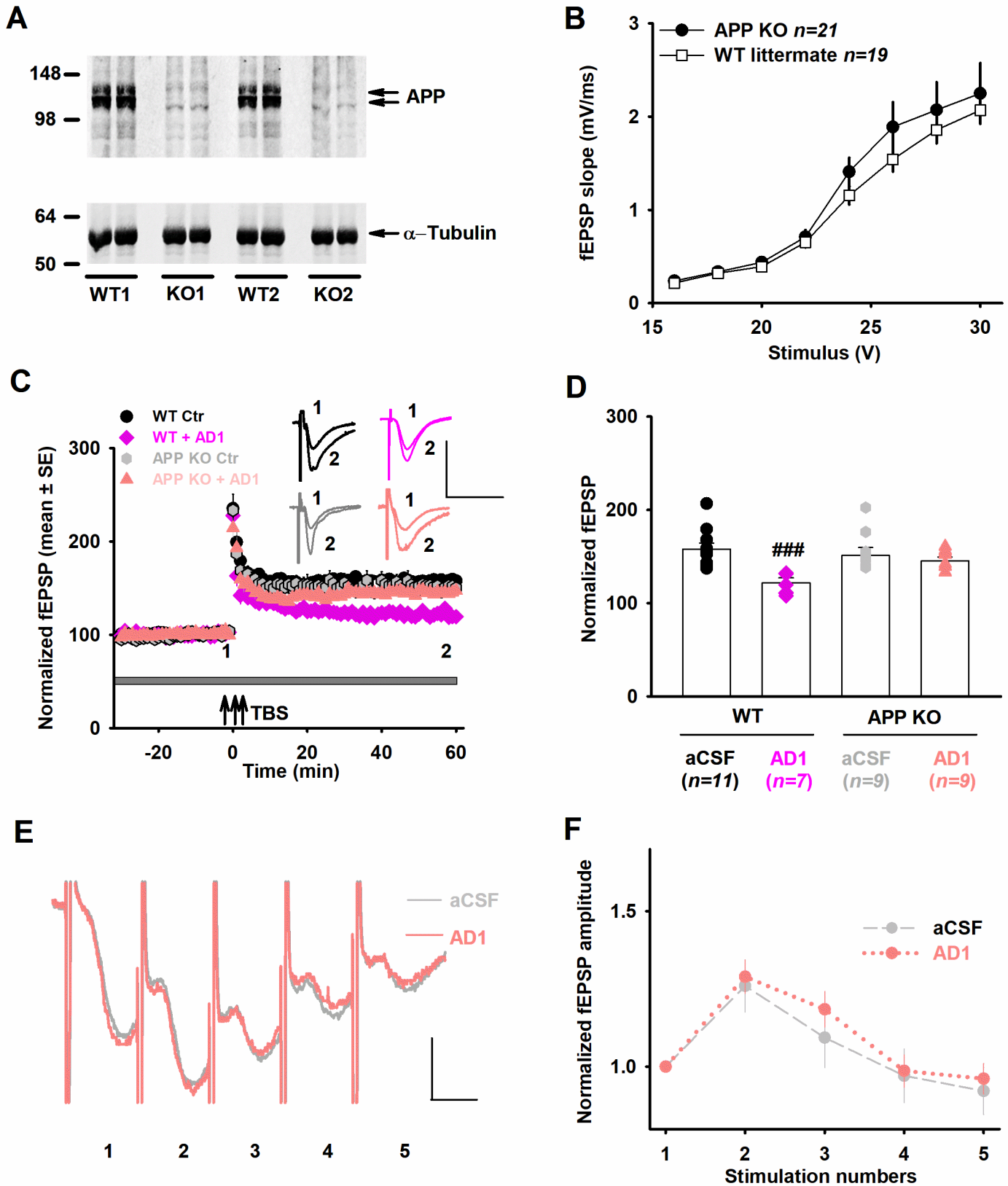


Figure 6: Characterization of the aqueous extract from AD2 brain, synthetic A β oligomers and a second APP KO mouse line.

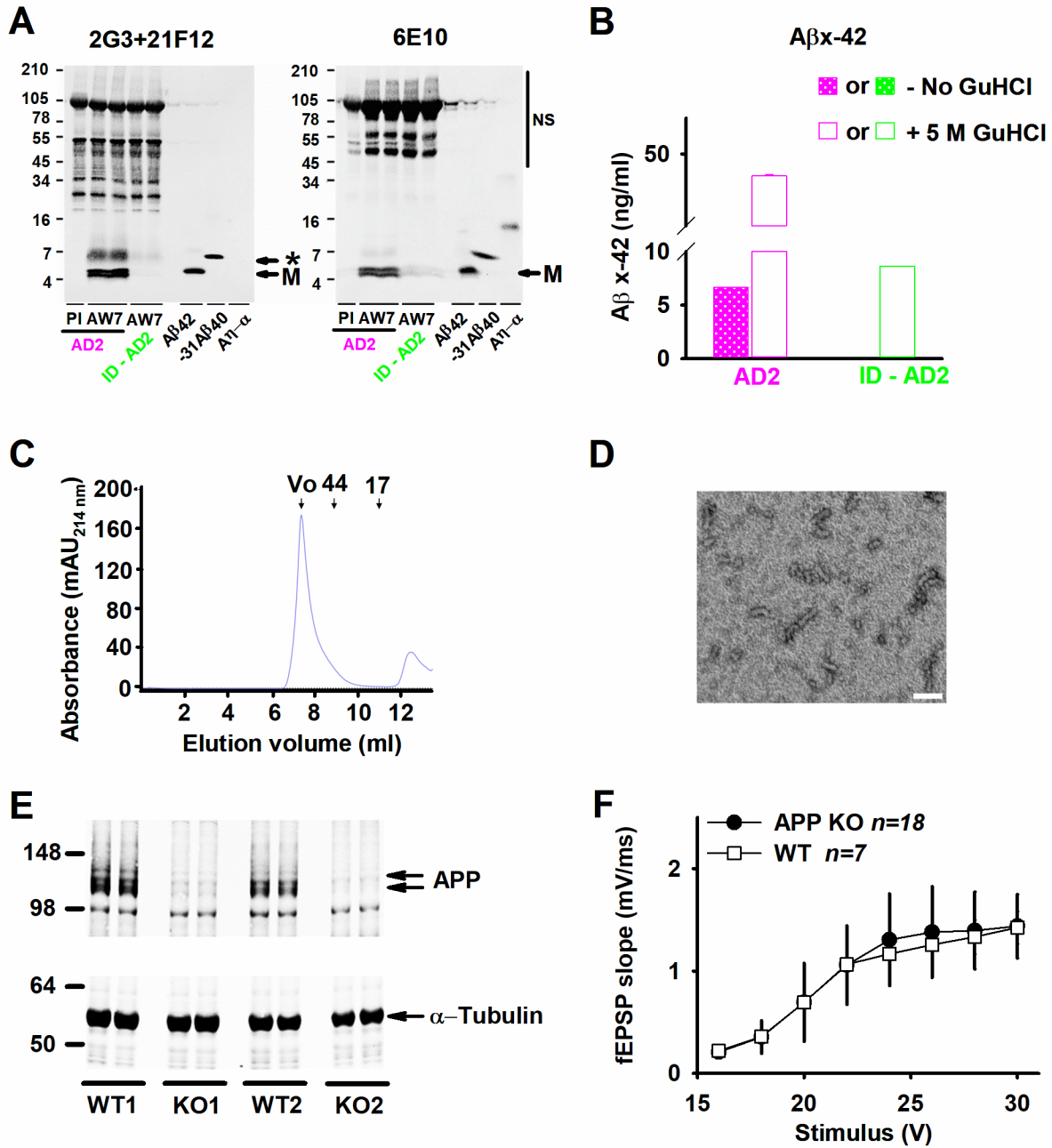


Figure 7: A second APP KO mouse line confirms that APP is required for the synaptic-disrupting activity of both AD brain and synthetic A β oligomers.

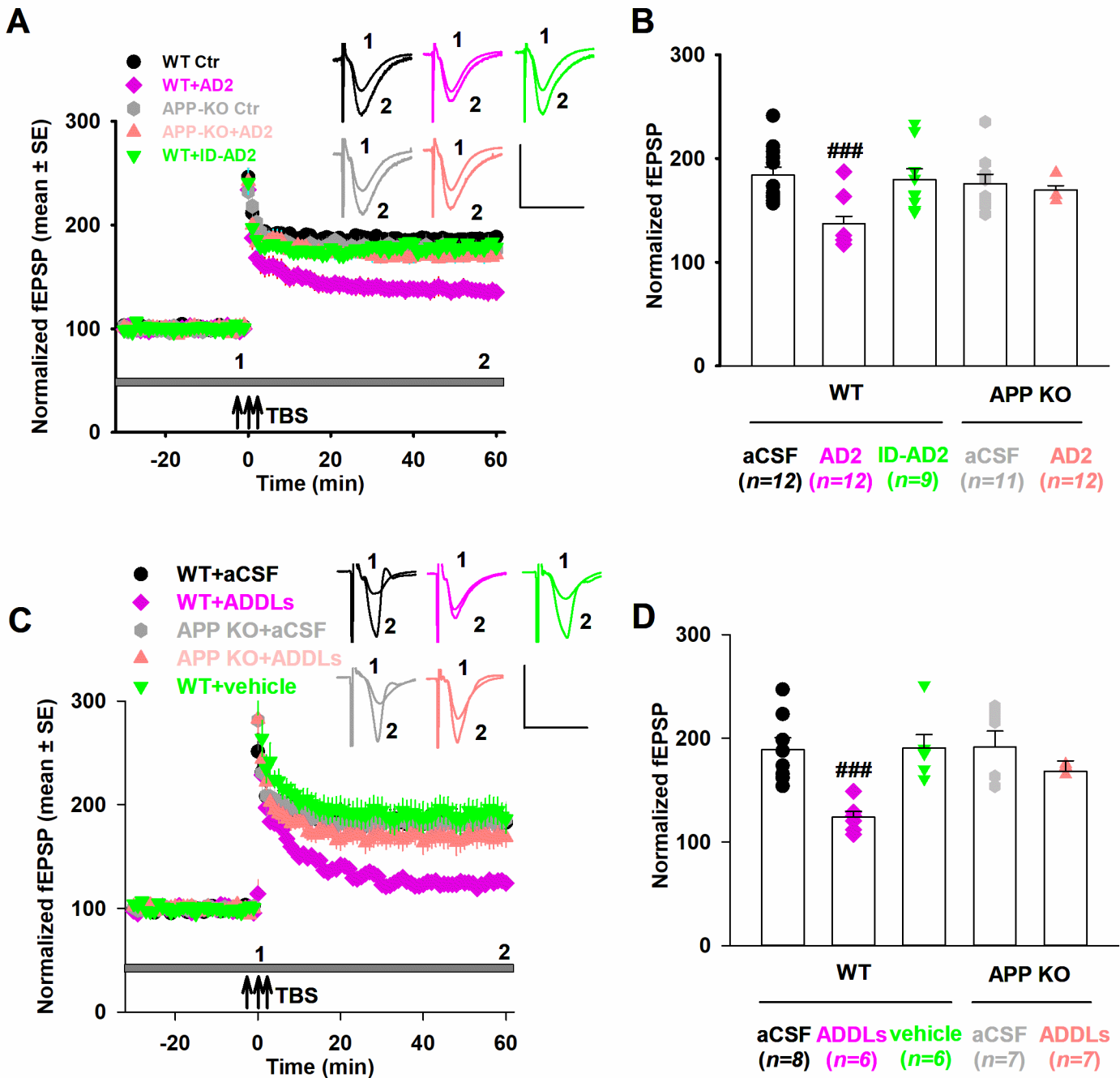


Figure 8: APP knock out occludes the effects of $A\beta$ -containing AD brain extract on both excitatory and inhibitory postsynaptic currents and rescues the disruption of E/I balance.

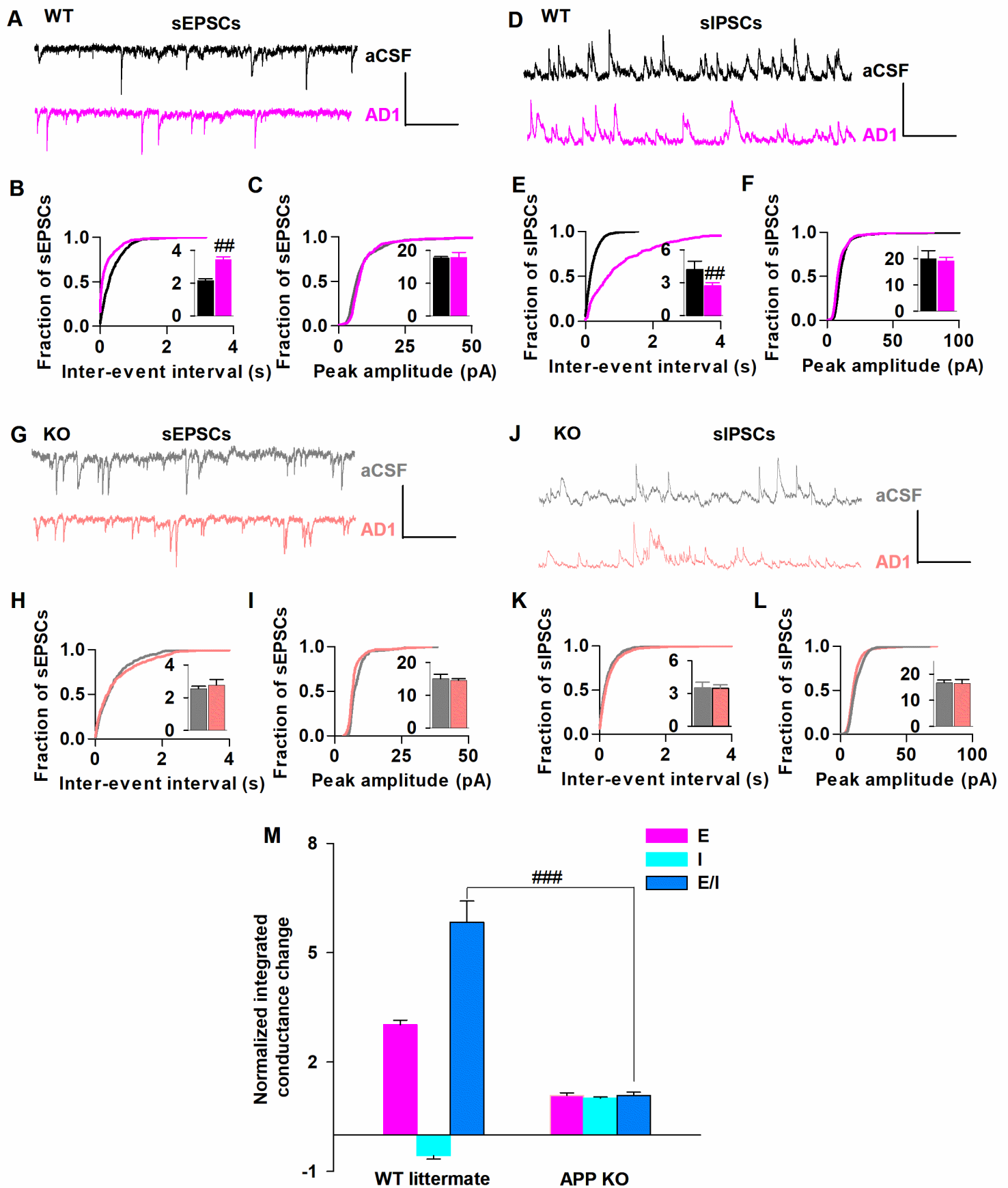


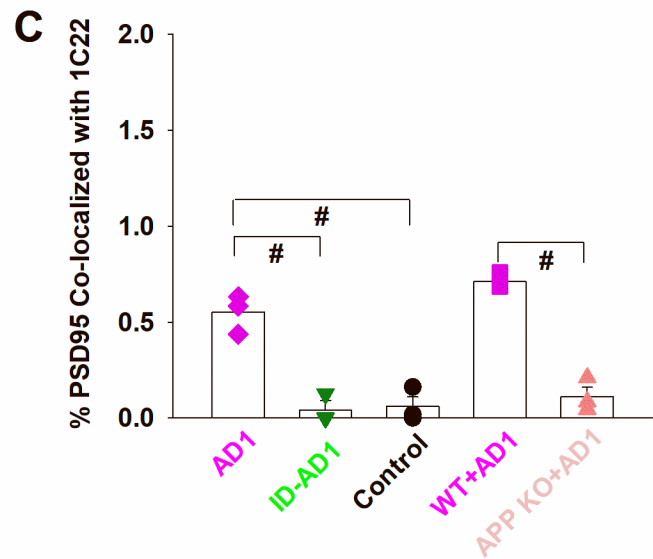
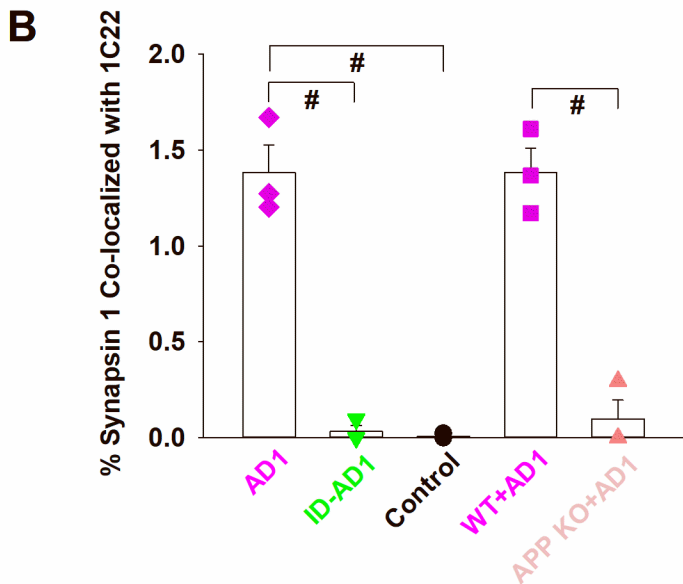
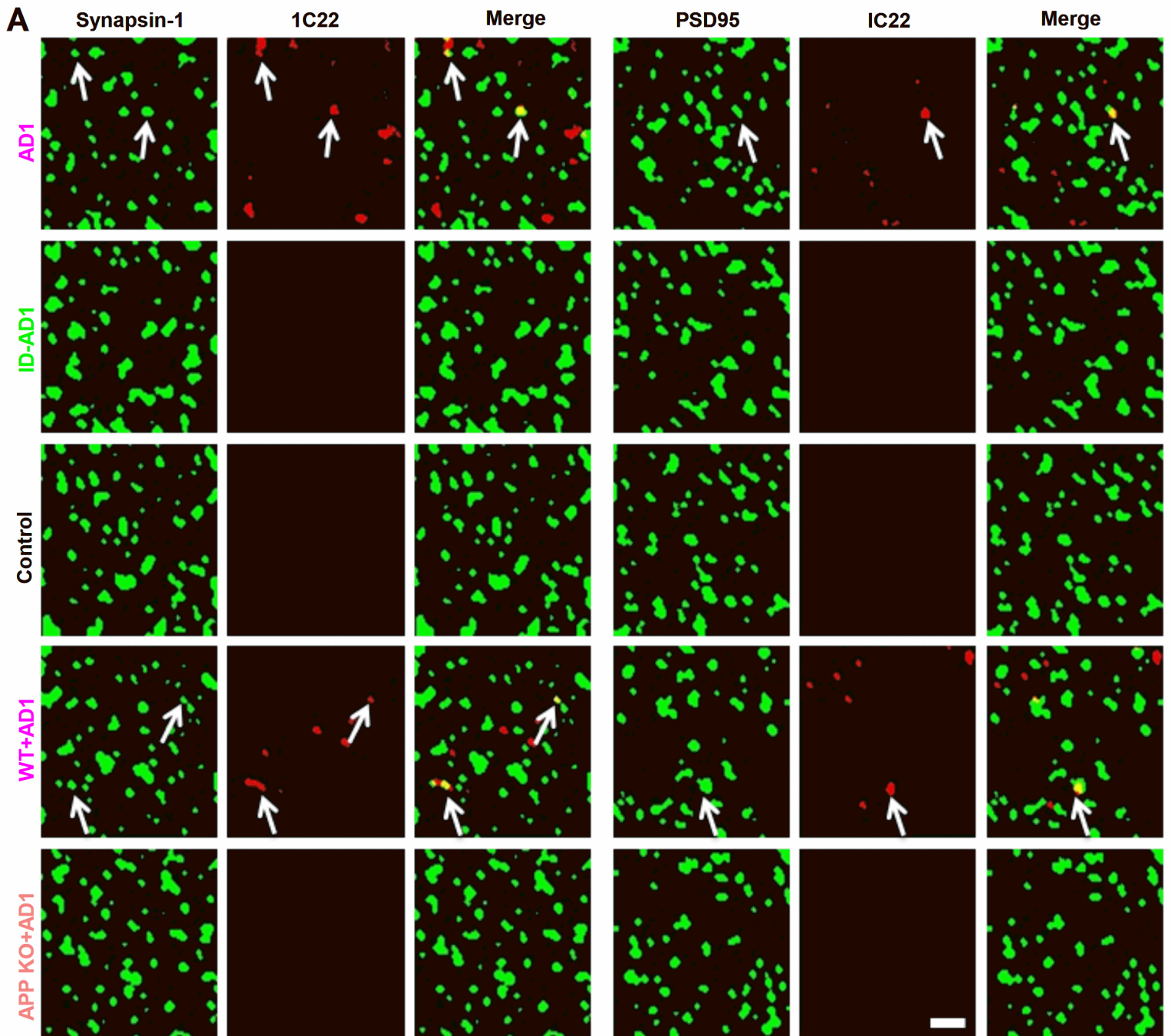
Figure 9: A β binding to synaptic terminals requires expression of APP.

Figure 10: APP expressing, but not APP lacking brain slices bind synaptotoxic A β .

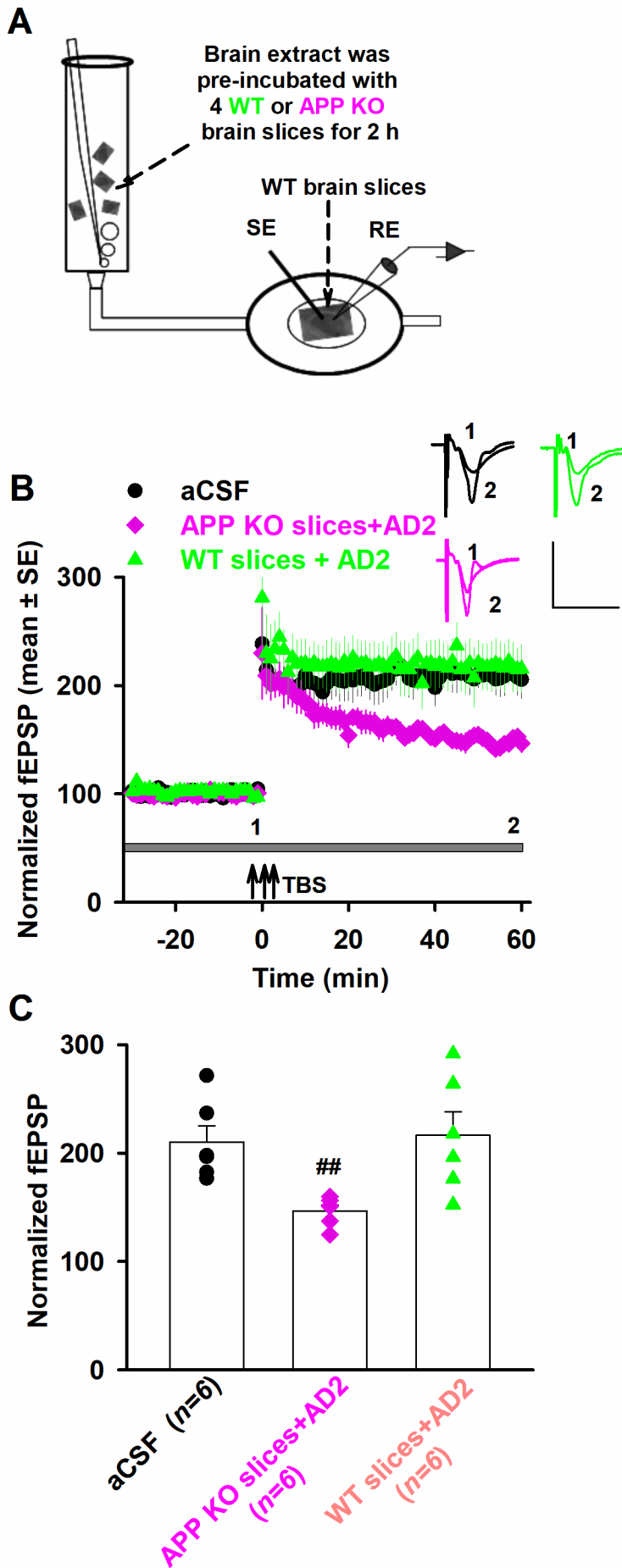


Figure 11: The level of APP expression influences the plasticity-disrupting activity of A β -containing AD brain extract.

